Volume 53 2013 No. 1 & 2

JOURNAL OF NATURAL SCIENCES AND MATHEMATICS

ISSN: 0022-2941
CODEN: JNSMAC

GOVERNMENT COLLEGE UNIVERSITY
LAHORE-54000, PAKISTAN

CONTENTS

Annual Subscription

Pakistan: Rs 250 Foreign Countries: US$ 40 Overseas Air Mail Charges: US$ 10

The Journal is published bi-annually
In April and October

Published by:
Riaz Ahmad for Government College University, Lahore, Pakistan.

Printed at:
PRIME Publishers.

JOURNAL OF NATURAL SCIENCES AND MATHEMATICS
INFORMATION FOR AUTHORS

1. TYPES OF PAPERS ACCEPTED

The Journal aims at publishing original research papers and the review papers from distinguished scientists on Mathematics, Physics,Chemistry and Computer Science.

2. SUBMISSION OF MANUSCRIPTS

Manuscripts should be submitted in duplicate to the Section Editor concerned. All papers are refereed. The decision of the Editorial Board regarding the acceptance and publication of the paper will be final.

3. PREPARATION OF MANUSCRIPT

3.1 Language and Style

All submissions should be in English, typed in double spacing on one side of the paper only with a left hand margin of at least 4 cm. Mathematical expressions must be carefully printed.Computer composed manuscript on C.D. in Microsoft Word is required for speedy publication.

3.2 Abstract

This should comprise a brief and factual summary of contents and should be suitable for direct use by abstracting journals. This will seldom require more than 200 words.

3.3 Section/Sub-Section Headings

Papers should be divided into sections / sub-sections and numbered as exemplified in the headings of this INFORMATION FOR AUTHORS.

3.4 References

References should be numbered consecutively in the text, e.g. "According to a recent theory [6]...it is well established [7]" and collected at the end of the paper in following style:

6. I. M. Ghauri and P. Feltham, J. Nat. Sci. Math., 26 (1986) 63.
7. W. Greiner and J. Maruhn, Nuclear Models, Springer-Verlag, Berlin, (1996).

3.5 Illustrations

Line diagrams must be drawn in black ink on white paper; original and two copies are required. Photographs or half-tone reproduction should be in the form of highly glazed prints. Figures are also acceptable in the form of jpg or tif format of 300 dpi. A separate list of captions for illustrations should be provided.

4. PROOFs

Only one set of proof is sent to the authors for correction.

PK ISSN 0022- 2941; CODEN JNSMAC
Vol. 53, (2013) PP 01-12

CHARACTERIZATION OF PULSED DC NITROGEN PLASMA USING OPTICAL EMISSION SPECTROSCOPY AND LANGMUIR PROBE

M. S. SHAH*, R. AHMAD, U. IKHLAQ AND S. SALEEM

Department of Physics, Government College University Lahore, Pakistan
*E-mail address: ms_shah_sgd@yahoo.com

(Received: March 10, 2014)

ABSTRACT: Nitrogen plasmas are generated by cost-effective 100 Hz pulsed dc electric power souse. Active species of nitrogen in plasma play key role in surface treatment. Optical emission spectroscopy and Langmuir probe are used to measure the plasma parameters. Measurements are carried out for various pressures (1, 1.5, 2 and 2.5 mbar) and powers (25, 50, 75 and 100 W). Optical spectra collected within the span range 300-900 nm. Electron temperature and electron density are evaluated by using intensity ratio of two atomic nitrogen lines (746.8 nm and 869.1 nm) and full width at half maximum (FWHM) of a Stark broadened line (746.8 nm) respectively. Langmuir probe is also used for determination of electron temperature, density, flux and velocity in plasma. It is found that value of these parameters decreases with increase of filling pressure and increases with source power. It is also found that more energetic electrons are produced at 1 mbar pressure for 100 W power and thus are responsible for enhanced plasma-reaction with surface treatment.

Keywords: Nitrogen plasma; 100Hz Pulsed dc, Langmuir probe, Optical emission spectroscopy.

1. INTRODUCTION

There is a growing interest in the study of ac and dc discharges for their applications in various industrial disciplines for surface modification, sputtering, etching, plasma assisted and plasma enhanced chemical vapor deposition. To use discharges, it is essential to have information about plasma and to have control on parameters. The processes and reaction rates occurring in plasma are generally dependent on density of charge particles and their energies [1]. In order to analyze the plasma–surface interaction, various kind of diagnostic tools have been employed. The different species present in plasma and plasma parameters, especially those involved directly in the surface treatment processes, have been studied by the electrical and optical plasma diagnostic tools such as electrostatic probe, optical emission spectroscopy (OES), Laser-induced fluorescence (LIF) and absorption spectroscopy, etc. [2]. There are two popular techniques for determining the plasma parameters: Optical emission spectroscopy and Langmuir probe measurements.

Optical emission spectroscopy is a popular technique to investigate glow discharges for identification of plasma species used in surface treatment. It is analysis of plasma light spectrum which is used for diagnosis and monitoring

plasma processes. From emitted spectral lines, spectral species can be identified by measuring intensities and wavelengths which provide information about physical and chemical processes in plasma. Purpose of optical emission spectroscopy is to obtained information as possible (like electron temperature Te and density ne) within the limits of spectra emitted from plasma in optical range. It is a non-invasive and established diagnostic technique with all necessary apparatus placed outside the chamber and has proved cost-effective and valuable in basic and applied science area [1-4].

In case of low-temperature and low-pressure plasmas, Langmuir probe gives reliable way to interpret results compared to other plasma diagnostics. It is possible to determine variety of parameters characterizing the plasma, such as electron temperature, density, velocity and flux etc. [5, 6]. The I-V characteristics obtained from Langmuir probe are mostly used for the measurement of plasma parameters. It is an invasive technique as the probe is inserted in plasma chamber through side port [3, 5].

In this work, optical emission spectroscopy along with Langmuir probe is used to analyze inter-electrodes plasma emerging from 100 Hz pulsed dc source. The effect on the plasma parameters is determined by varying pressure and power in order to optimize conditions for surface treatment. This cost-effective study can contribute for many applications.

2. EXPERIMENTAL SETUP

Experiment is performed between two capacitively coupled circular stainless steel electrodes spacing 3 cm, having 14 cm diameter and thickness of 2 cm each. Electrodes are covered with ceramic to avoid the additional discharge and are fitted in an evacuated (1×10^{-2} mbar) vacuum chamber shown in Fig. 1. The pressure is measured using capsule type vacuum gauge (0–25 mbar) along with the Pirani gauge. A 100 Hz pulsed dc power output using ac power (50 Hz) source and bridge rectifier circuit is applied through inductive load to the top electrode, whereas, bottom electrode is grounded. Inlet and outlet valves are adjusted so as to maintain the required pressure in the chamber.

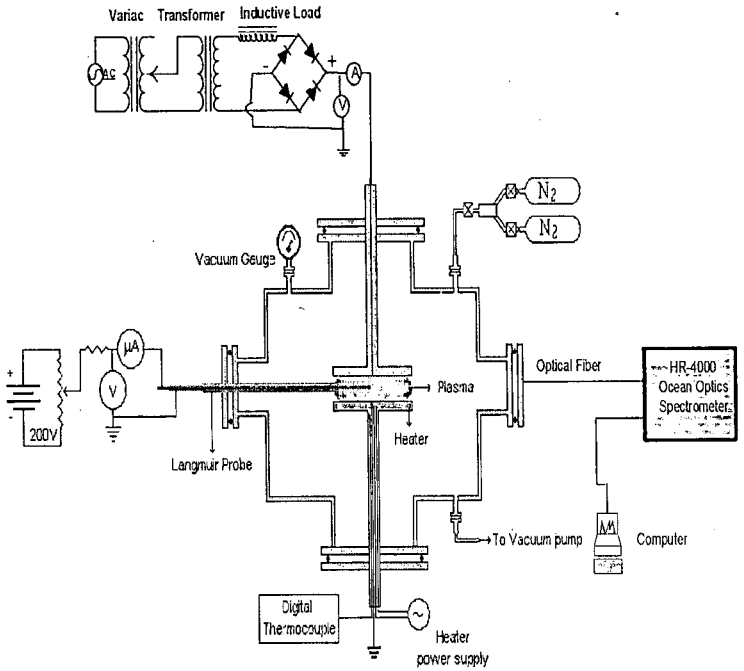

Fig. 1: Langmuir probe and OES characterization of plasma using 100 Hz pulsed dc.

Plasma diagnostics:

(a) Spectrometric diagnostic

In nitrogen plasma, active species are investigated with optical emission spectroscopy, using a quartz optical fiber. The optical diagnostic system consists of optical emission spectrometer HR-4000. It is coupled with quartz optical fiber which is positioned at center of the side port of the chamber and detects plasma glow above the substrate. Wave length of spectrometer is calibrated using argon-mercury lamp. The optical signal is detected by optical fiber on the computer using the spectrometer in spectral range of 300-900 nm. The plasma active species are then analyzed in plasma induced optical emission using a computer controlled system.

(b) Probe diagnostic

Langmuir probe is a small metallic insulated wire (electrode) except at the tip, which is inserted into plasma. Material used for probe wire is tungsten because of their high melting point. The probe assembly consists of an exposed tungsten wire of diameter 0.2 mm and length 3 mm, sealed in a Pyrex glass tube. The wire length is much greater than the wire diameter so that edge effects are negligible. The conducting wire inside the glass tube is covered with an earthed copper web

shield. The probe can be positioned in plasma and swept radially and axially across the chamber through one of the ports windows. I-V characteristics of the probe are measured for dc bias voltages swept from -100 V to +100 V. Langmuir probe measurements are also recorded for the same parameters of pressure (1, 1.5, 2 and 2.5 mbar) at constant power (100 W).

3. RESULTS AND DISCUSSION

Typical emission spectrum of nitrogen is shown in the Fig. 2. The prominent band system of spectral lines of nitrogen as well as sputtered Fe are observed at 1 mbar pressure and the input power of 100 W. The molecular band is studied with discharge parameters as those belonging to first negative system $[N_2^+(B\ ^2\sum_u^+) \rightarrow N_2^+(X\ ^2\sum_g^+)]$ which is represented neutral excited molecules N_2^+. The $N_2^+(B\ ^2\sum_u^+)$ states are mainly produced by electrons and are quickly disappeared in afterglow due to the N_2^+-electron recombination. Intense peak is found that comes from the first negative system, which is characteristic of N_2 negative glows [2,7], resultant to electronic transition from ground vibrational level of $B\ ^2\sum_u^+$ state to ground vibrational level of $X\ ^2\sum_g^+$ state. This system is observed in the negative column (as its name indicates) of nitrogen discharge and strongly emits at 391.4 nm and 427.8 nm in negative glow [8]. Emission intensity of first negative band head is proportional to population of $N_2^+(B\ ^2\sum_u^+)$ state. Emission intensity of selected line characterizes sputtering of cathode material, which is caused mainly by bombardment of the positive ions. Sputtered Fe atoms arrive in glow discharge and are then subjected to collisions with electrons and plasma species. Excitation collisions and subsequent decays emit characteristic photons of Fe atoms [9]. Intensity of these emitted photons of characteristic wavelength gives concentration of the Fe atoms in the discharge.

Fig. 2 shows the emission lines intensity ratio of active species of nitrogen versus input power. It is found that intensity ratio increases rapidly by increasing input power, explained as: when input power increases, electrons attain sufficient energy to cause excitation and ionization of the nitrogen molecules through inelastic collisions. Energy of ejected electrons from cathode increases the excitation cross-section due to bombardment of positive ions which decreases with increase in electron energy above excitation threshold of N_2 [10].

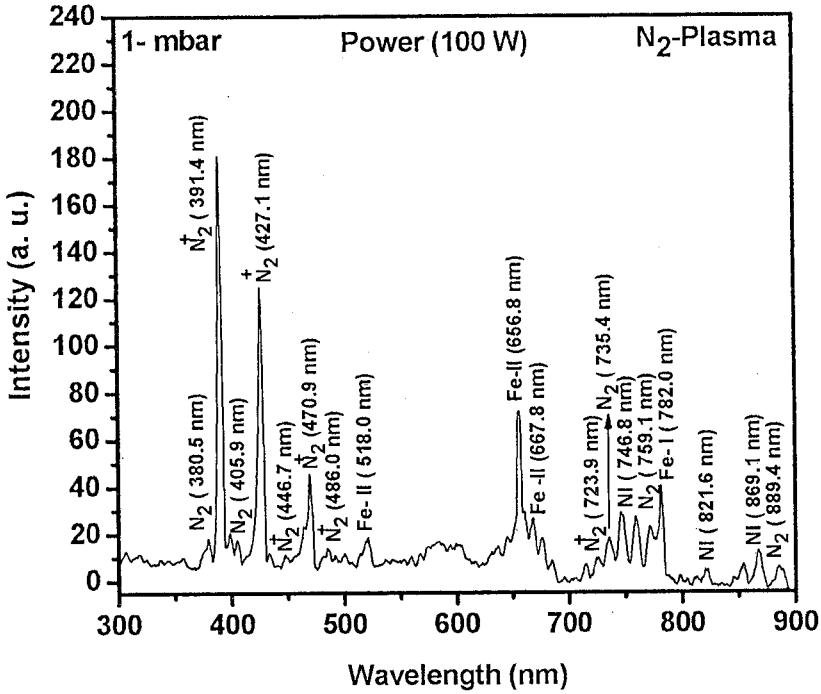

Fig. 2: A typical optical emission spectrum of nitrogen plasma at 1 *mbar* pressure and 100 W power.

Fig. 3 shows the intensity ratio of lines with filling pressure. It is found that this ratio decreases with the increase of pressure. Reduction with filling pressure is explained as follows: At low pressure, the density of species of nitrogen is small and mean free path of free electrons is larger which results in gain of energy by dc electric field. However, by increasing pressure this path is not large enough to accelerate free electrons. Therefore, emission intensities decrease and collisions among plasma species and electrons increase causing increase in species temperature by lowering electron temperature and hence high energy tail of electron energy distribution is quenched [10].

In low pressure plasma electron temperature and density can be measured spectroscopically. Electron temperature can be measured by using line intensity ratio method by considering the integrated intensity ratio of two spectral lines belonging to the same atomic species [1,11,12]. The formula is given by,

$$T_e = \frac{E_2 - E_1}{k}\left[\ln\left(\frac{A_2 g_2 I_1 \lambda_1}{A_1 g_1 I_2 \lambda_2}\right)\right]^{-1}$$

where $(E_1 - E_2)$ is the energy difference of two spectral lines, I_1 is the integrated line intensity of one line. The respective values of specifications used for two lines are given in table 1.

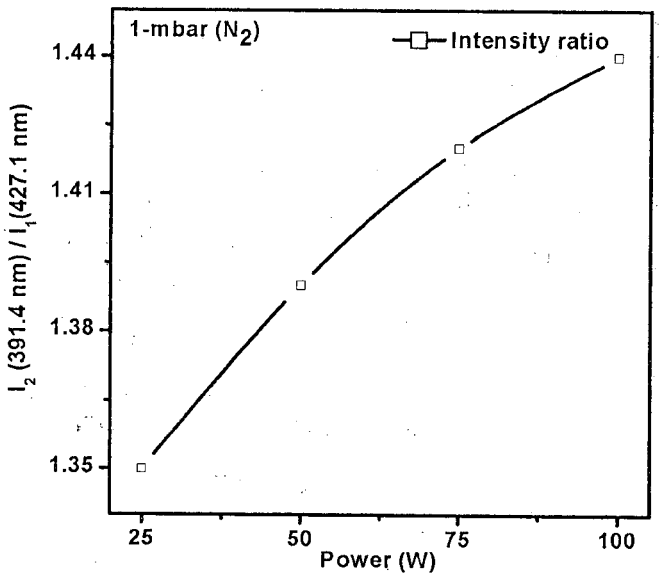

Fig. 3: Variation in intensity ratio of the emission lines (391.4 nm and 427.1 nm) with power.

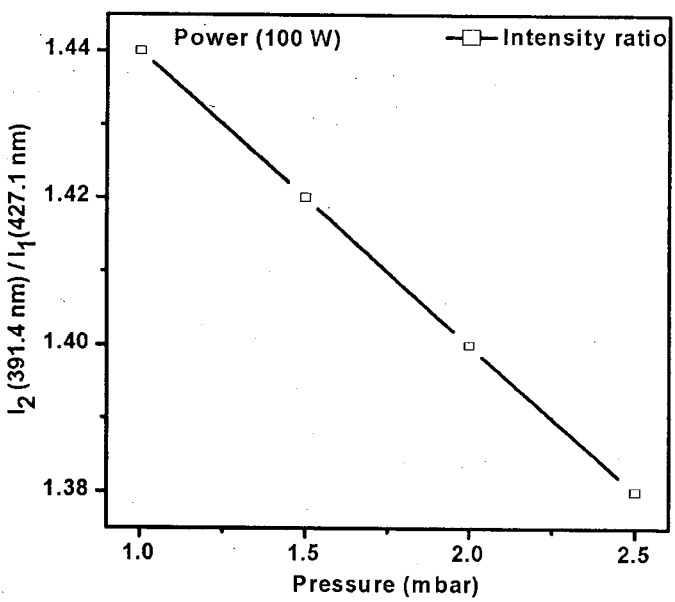

Fig. 4: Variation in intensity ratio of the emission lines (391.4 nm and 427.1 nm) with pressure.

Table 1: Nitrogen spectral lines for electron temperature measurements

wavelength Statistical	Excitation	energy	Transition
(nm)	(eV)	Probability (A)	Weight (g)
746.8	11.90	1.68 x $10^7 s^{-1}$	4
869.1	11.75	1.83 x $10^7 s^{-1}$	20

Electron number density is determined by using Stark broadening technique. It is known that the full width at half maximum (FWHM) of a Stark broadened line $\Delta\lambda_{1/2}$ is related to electron density as [11],

$$\Delta\lambda_{1/2} = 2W(n_e \times 10^{-16})$$

where W is the electron impact parameter and n_e is electron density. A typical Stark broadened line profile is almost the Lorentzian.

Electron number density is evaluated by using Stark broadening technique with selected line (746.8 nm) of nitrogen. The full width at half maximum (FWHM) values of a Stark broadened line $\Delta\lambda_{1/2}$ for different parameters corresponding values of electron impact parameter W are given in table 2 [11],

Table 2: To calculate electron density, half width of spectral Line (λ =746.8 nm) using electron impact parameter (W=0.0475) for nitrogen plasma.

Input power (W)	FWHM ($\lambda_{1/2}$)	Pressure (mbar)	FWHM ($\lambda_{1/2}$)
25	5.84	1.0	7.88
50	7.12	1.5	6.61
75	7.37	2.0	5.50
100	7.88	2.5	5.01

Fig. 5 and 6 illustrate evolution of electron temperature and density versus input power as well as filling pressure. Results predict that with increasing source power, electron temperature as well as electron density increase due to inelastic collisions of electrons, attaining enough energy which causes the excitation and ionization of nitrogen molecules. The energy of secondary electrons increases excitation cross-section and decreases with electron energy.

It is found that with increasing filling pressure electron temperature and density decreases. At higher pressures, mean free path is not large enough to accelerate free electrons. Because collisions among plasma species and electrons increase causing increase in species temperature by lowering electron temperature and hence high energy tail of electron energy distribution is quenched, suggesting that number of energetic electrons at lower pressure is reduced [10].

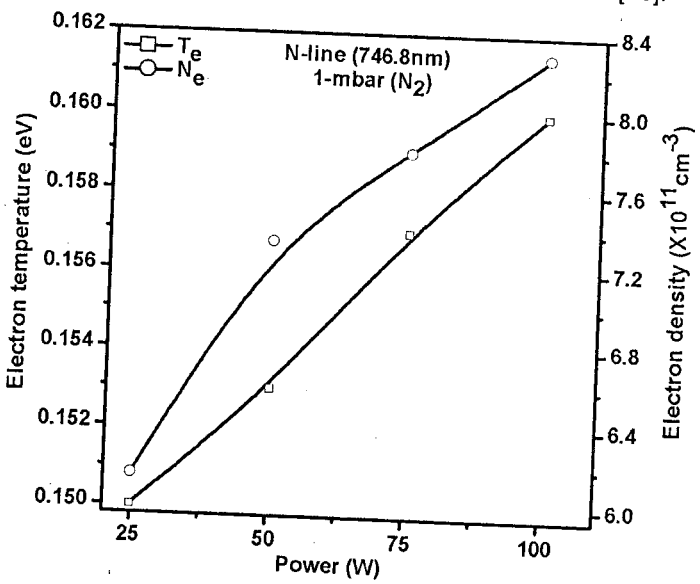

Fig. 5: Variation of electron temperature and density versus power using OES.

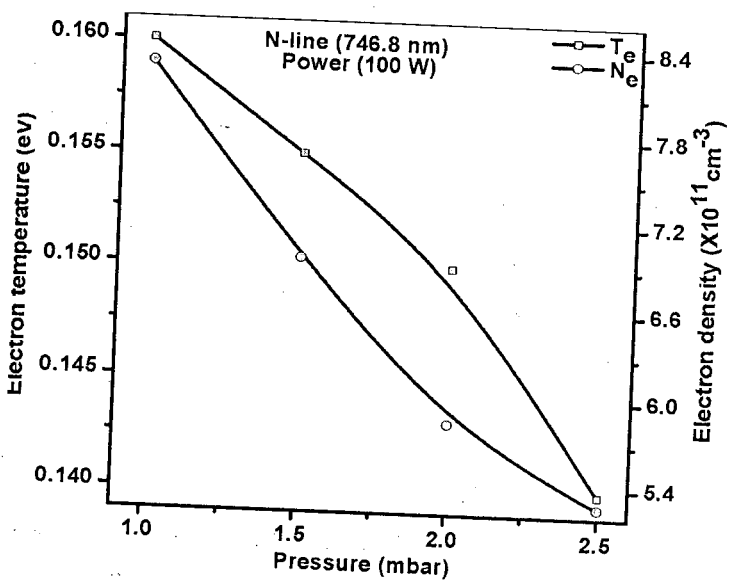

Fig. 6: Variation of electron temperature and density versus pressure using OES.

Langmuir probe measurements of electron temperature and density [1,3,13] are in Fig. 7, which shows that electron temperature and density decreases with the

increase of pressure as explained above. It is known that measured electron temperatures from Langmuir probe and spectroscopic technique have shown difference. The Langmuir probe normally determines higher temperature which may be due to the quick contamination (i.e. electrons, ions or impurities in plasma) of initially cleaned surface of probe. However, presence of this contamination layer reduces the amount of current collected from the plasma. Hence, Langmuir probe shows higher values as compared from spectroscopic measurements [1].

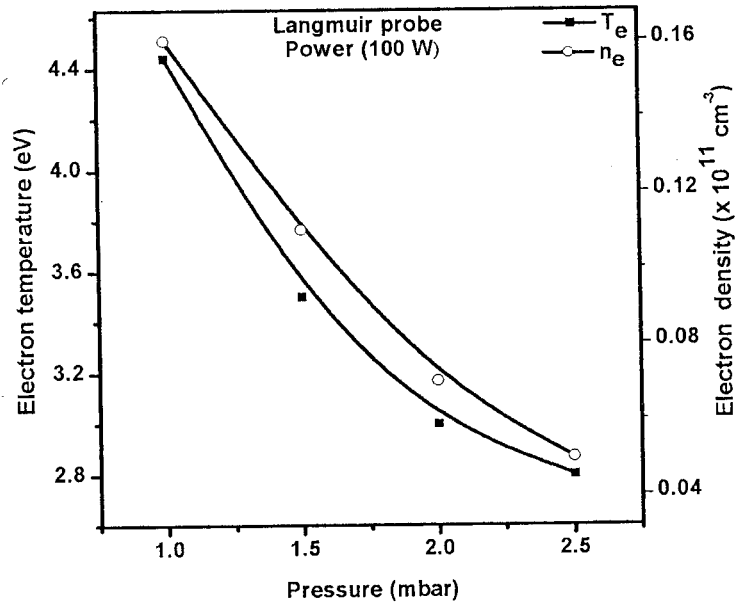

Fig. 7: Variation of electron temperature and density versus pressure using Langmuir probe.

Average thermal velocity of electrons in plasma is calculated using following equations [3, 14],

$$v_e = \left(\frac{8kT_e}{\pi m_e} \right)^{1/2}$$

where v_e is the electron velocity.

Fig. 8 indicates the variation of average thermal velocity of electrons versus pressure. The electrons velocity is measured with both OES and Langmuir probe exhibit decrease in velocity of electrons with filling pressure, which is found to be the multiple order of $10^6 ms^{-1}$. Flux of the nitrogen particles striking on a unit surface area in a unit time increment [14] determines the maximum rate at which the gas can react with the surface, causing increase of local temperature.

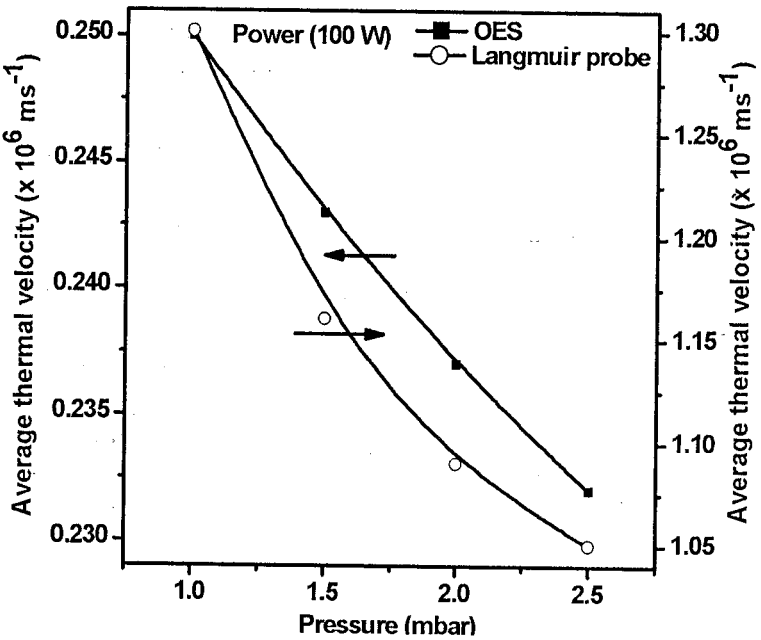

Fig. 8: Variation of OES and Langmuir probe measurements of average thermal velocity of electrons versus pressure.

Electron flux (Γ_e) can be determined using equations [5, 14].

$$\Gamma_e = \frac{1}{4} n_e v_e$$

The flux of nitrogen particles striking a surface determines the maximum rate at which the gas can react with the surface. The term flux describes the number of particles impinging on a unit surface area in a unit time increment.

Figure 9 shows electron flux variation versus pressure also measured with both diagnostics. It is observed that flux of electrons decreases with filling pressure, which is found to be the multiple order of $10^{20} m^{-2}$. Hence, it is found that more energetic atoms/ ions are produced at $1\,mbar$ pressure and $100\,W$ power. Therefore, these conditions are more favorable for surface modification like nitriding etc.

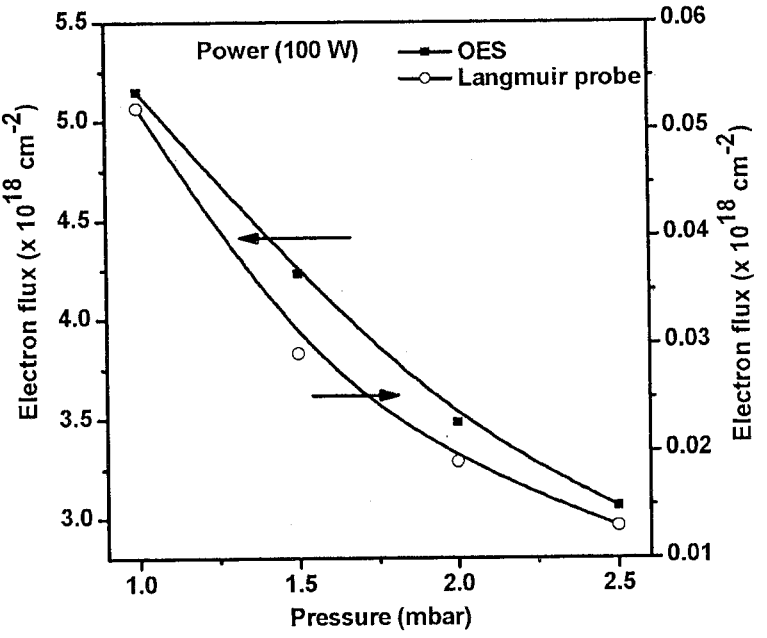

Fig. 9: Variation of OES and Langmuir probe measurements of electron flux versus pressure.

4. CONCLUSIONS

Nitrogen plasma analysis is carried out to optimize the parameters using optical emission spectroscopy as well as Langmuir probe. Plasma is energized by 100 Hz pulsed dc source for surface treatment. Using optical emission spectroscopy, emission lines of atomic, ionic and molecular nitrogen species and Fe are detected. Around cathode, the first negative system of nitrogen with a strong emission is observed. Electron temperature, electron density, flux as well as their velocities in plasma are evaluated in terms of their dependence on the filling pressure and input power. It is found that concentration of active species is affected by the power and pressure and attains their highest values at 1mbar pressure and 100 W power.

REFERENCES

1. A. Qayyum, M. Ikram, M. Zakaullah, A. Waheed, G. Murtaza, R. Ahmad, A. Majeed, N. Khattak, A. D. Mansoor, K. K. A. Chaudhry, Inter. J. Modern Phys., B 17 (2003) 2749.
2. Y. M. Kim, U. K. Jong, J. G. Han, Surf. Coat Technol., 151 (2002) 227.

3. M. Nisha, K. J. Saji, R. S. Ajimsha, N. V. Joshy, M. K. Jayaraj, J. Appl. Phys., 99 (2006) 033304.
4. M. A. Naveed, N. U. Rehman, S. Zeb, S. Hussain, M. Zakaullah, Eur. Phy. J. D, 47 (2008) 395.
5. M. S. Shah, M. Saleem, R. Ahmad, M. Zakaullah, A. Qayyum, G. Murtaza, J. Mater. Process. Technol., 199 (2008) 363.
6. T. K. Popov, M. Dimitrova, F. M. Dias, Vacuum, 76 (2004) 417.
7. S. Gredelj, A. R. Gerson, S. Kumar, G. P. Cavallaro, Appl. Surf. Sci., 174 (2001) 240.
8. M. J. Baldwin, S. C. Haydon, M. P. Fewell, Surf. Coat. Technol., 97 (1997) 97.
9. A. Qayyum, R. Ahmad, A. Waheed, M. Zakaullah, Eur. Phys. J. Appl. Phys., 32 (2005) 45.
10. A. Qayyum, S. Zeb, M. A. Naveed, S. A. Ghauri, A. Waheed, M. Zakaullah, Plasma Devices Oper., 14 (2006) 61.
11. M. Hanafi, M. M. Omar, Y. E. E-D. Gamal, Radiation Phys. & Chem., 57 (2000) 11.
12. N. K. Podder, J. Johnson, C. T. Raynor, S. D. Loch, C. P. Balance, M. S. Pindzola, Physics of Plasma, 11 (12) (2004) 5436.
13. A. Grill, Cold Plasma in Material Fabrication: Fundamentals to Applications IEEE Press, New York (1994).
14. D. T. K. Kwok, M. M. M. Bilek, D. R. Mckenzie, T. W. H. Oates and K. Chu Paul, IEEE Transactions on Plasma Sci., 32 (2) (2004) 422.

PK ISSN 0022- 2941; CODEN JNSMAC
Vol. 53, (2013) PP 13-22

AEROSOL CONCENTRATION IMPACTS ON RAINFALL IN PAKISTAN

A. R. KHAN*[1], K. REHMAN[2] AND M. MANZOOR[3]

[1]University Malaysia Sabah, Malaysia
[2]University of Windsor, Ontario, Canada
[3]Govt. College for Women, Banghbanpura, Lahore, Pakistan
*E-mail address: aaliya.rehman@gmail.com

(Received: January 01, 2014)

ABSTRACT: Aerosol physical and optical properties were measured at two locations in Central Pakistan. The first set of measurements were done at Lahore, while the second at Jhelum, about 194 km North of Lahore, with data taken in 2011 and 2012. At both stations, the average aerosol concentrations during the monsoon were decreased by 40–75% compared to the pre-monsoon average concentrations, with decrease varying with the total local rainfall. In Jhelum, the monsoon season removed particles from all size classes, due to a combination of rain scavenging and activation to cloud and mountain fog droplets. The aerosol columnar properties, which were measured in Lahore, showed a somewhat different seasonal behavior compared to the surface measurements, with the aerosol optical depth increasing to an annual maximum in the early monsoon season. The present investigation has that AOD was high in monsoon season and it was low during winter season.

Keywords: Aerosol optical depth, Rainfall, Cloud parameters, Monsoon, COD.

1. INTRODUCTION

Asian Summer Monsoon and its importance are quite well known to the Asians. In recent years it has become evident that aerosols may influence the precipitation patterns of the Summer Monsoon. This may be especially important in Southern Asia, since the area suffers from an intense and persistent particulate pollution called the "brown cloud" [1-2]. The influence of the brown cloud on monsoon patterns has been investigated in numerous studies; the most famous work on this being the so-called "Elevated Heat Pump" hypothesis (EHP) [4]. According to the EHP hypothesis, absorbing aerosols accumulate against the southern slopes of the Himalayas in the pre-monsoon season, thereby modulating the tropospheric temperature gradient. The reinforced meridional temperature gradient then leads to an early onset of monsoon and intense rainfall during June and July.

A wide range of measurements shows that anthropogenic aerosol often alter clouds and their optical properties [5-9]. In the last decade, among Asian monsoon countries such as China, Pakistan and India, the aerosol problem is becoming increasingly acute In 2003, Sindh province was badly affected when above normal monsoon rainfall caused flooding in the province; urban flooding also hit Karachi where two days of rainfall of 284.5 mm (11.20 in) created havoc

in the city, while Thatta district was the worst hit where 404 mm (15.9 in) rainfall caused flash floods in the district. At least 484 people died and some 4,476 villages in the province were affected [10-12]. In 2007, Khyber-Pakhtunkhwa, Sindh and coastal Balochistan were badly affected due to monsoon rainfall. Sindh and coastal Balochistan were affected by Cyclone Yemyin in June and then torrential rains in July and August, while Khyber-Pakhtunkhwa was affected by melting glaciers and heavy rainfall in July and August. At least 130 people died and 2,000 were displaced in Khyber-Pakhtunkwa in July and 22 people died in August, while 815 people died in Balochistan and Sindh due to flash floods [13]. In 2010, almost all of Pakistan was affected when massive flooding caused by record breaking rains hit Khyber-Pakhtunkhwa and Punjab. The number of individuals affected by the flooding exceeds the combined total of individuals affected by the 2004 Indian Ocean tsunami, the 2005 Kashmir earthquake and the 2010 Haiti earthquake [14]. At least 2,000 people died in this flood and almost 20 million people were affected by it [15]. In September 2011, at least 361 people were killed, some 5.3 million people and 1.2 million homes affected as well 1.7 million acres of arable land inundated when massive floods sweeped across the province of Sindh as a result of monsoon rains [16]. In September 2012, more than 100 people died, and thousands of homes destroyed, with thousands of acres of arable land affected when intense rainfall battered Khyber Pukhtunkhwa, Southern Punjab and Upper Sindh [17].

It has been estimated that aerosol may reduce up to 10% of the seasonal mean solar radiation reaching the Earth's surface at various regions of the globe, producing a global cooling effect that masks the global warming [18]. The aerosols with several ionic and carbonaceous components along with highly enriched heavy metals could interact with the fresh or less polluted aerosols of mostly marine origin and thus could degrade the forest/marine air quality [19]. The present study is the new endeavor to this region by using local observations to analyze the role of aerosol on the variation in the rainfall during monsoon season for two different years in two cities of Pakistan.

2. MATERIAL AND METHOD

Site Description

LAHORE

The first measurement station was located at Lahore [20] (31°15′—31°45′ N and 74°01′—74°39′ E) Figure 1. The Ravi River flows on the northern side of Lahore. Lahore city covers a total land area of 404 km² and is still growing. Lahore features a hot semi-arid climate (with rainy, long and extremely hot summers, dry

and warm winters, a monsoon and dust storms. The weather of Lahore is extreme during the months of May, June and July, when the temperatures soar to 40–48 °C. From late June until August, the monsoon seasons begins, with heavy rainfall throughout the province of Punjab. The city's highest maximum temperature was 48.3 °C recorded on 30th May, 1944 [20]. And 48 °C was recorded on June 10, 2007. At the time the meteorological office recorded this official temperature in the shade, it reported a heat index in direct sunlight of 55 °C. The lowest temperature recorded in Lahore is −1 °C recorded on 13 January 1967. The highest rainfall in the city recorded during 24 hours is 221 mm (8.7 in), which occurred on 13 August. 2008. The city on 26 February 2011, received heavy rain and hailstorm measuring 4.5 mm, which carpeted several roads and sidewalks with measurable hail for the first time in the climatic history of Lahore.

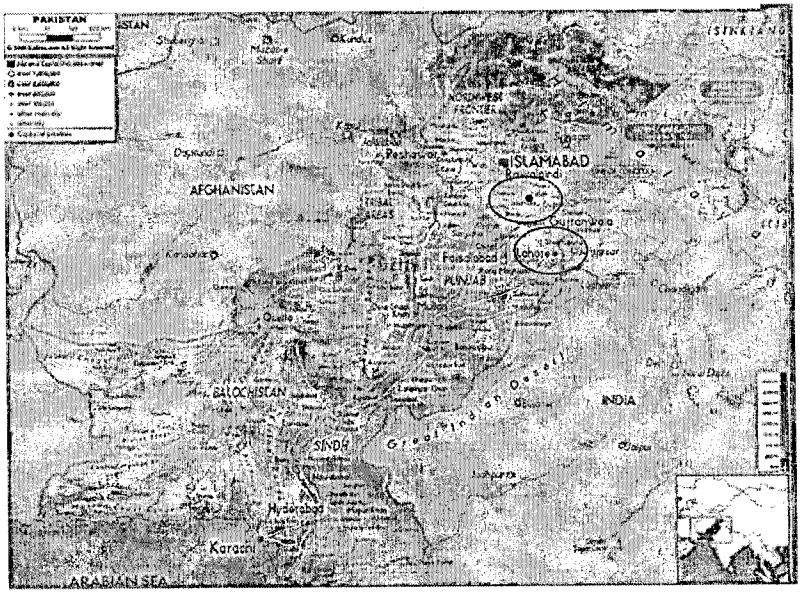

Fig. 1: The two measurement sites were Lahore and Jhelum

JHELUM

The second measurement site was located in Jhelum [21] (32°56′ North latitude and 73°44′ East) Figure 1. The population of the Jhelum city (proper) is about 188,800(2012) and it is the 32nd largest city of Pakistan with respect to population. Population Density is 261/km. Population Growth Rate is 1.51 which is very low as compared to other urban areas of Pakistan. Jhelum has a humid subtropical climate and is extremely hot and humid in summer, and warm and generally dry in winter. The maximum recorded temperature in the pre-monsoon season of April to June is 49.2 °C, whereas in winter the minimum

temperature recorded is −0.6 °C. Average annual rainfall is about 850 mm (33 in) which is much below the required quantity given the extremely high evaporation levels.

INSTRUMENTS

The parameters measured at Lahore included the particle number size distribution from 10nm to 800nm (DMPS), PM2.5 and PM10 concentrations (on-line beta-attenuation analyzers), aerosol scattering coefficient (Nephelometer at 525nm), black carbon concentration/absorption coefficient (7-wavelength Aethalometer) and meteorological parameters. All instruments sampled from a single sampling line (except the particle mass monitors which each had their own inlets), with a PM2.5 inlet located at about 5m above ground level and about 2m above the roof of the station building.

3. RESULTS AND DISCUSSION

Annual aerosol optical depth descriptive statistics has been given in the Table 1. Annual mean values of Aerosol optical depth were obtained by taking the daily mean values of AOD from 2011 to 2012. It has been observed that high burden of aerosol mass in polluted regions may resulted in higher AOD [22]. Factors such as overall pollutant load, atmospheric particulate matter concentration and sand along the road sides, all cumulatively contribute the continuous aerosol loading in the urban atmosphere of the city [23-27].

Table 1. Pre-monsoon, monsoon and post-monsoon average aerosol properties in Lahore, ± denotes standard deviation calculated from the hourly data.

Year	*Lahore*	*Abs coeff.* mm^{-1}	*Scat coeff.* mm^{-1}	N_{tot} cm^3	*N <25nm* cm^3	*N25<d <75nm* cm^3	*N >75nm* cm^3
2011	Pre	26.7±16.6	127.7±116.8	6401±4791	370±680	2200±1800	3795±3448
	Monsoon	6.9±4.9	74.1±60.3	3244±1819	119±169	1266±781	1929±1222
	post	18.3±11.4	31.5±26.5	2124±1234	156±248	777±464	1258±721
2012	Pre	25.7±16.6	128.7±119.8	6395±4841	368±685	2176±1831	3824±3448
	Monsoon	6.9±4.9	74.1±60.3	3244±1819	119±169	1266±781	1929±1222
	post	18.3±11.4	31.5±26.5	2124±1234	156±248	777±464	1258±721

Table 2. Pre-monsoon, monsoon and post-monsoon average aerosol properties in Jehlum, ± denotes standard deviation calculated from the *hourly data.*

Year	*Jhelum*	*Abs coeff.* mm^{-1}	*Scat coeff.* mm^{-1}	N_{tot} cm^3	*N <25nm* cm^3	*N25<d <75nm* cm^3	*N >75nm* cm^3
	Pre	60.8±49.7	312.7±253.2	4613±2531	274±581	1715±1230	2976±1534
2011	Monsoon	28.6±26.9	56.8±40.6	2023±876	54±56	730±323	1228±639
	post	109.0±59.9	1235.5±1291.2	25860±11707	1950±4046	6904±4299	1696±9486
	Pre	25.8±16.7	96.7±57.5	5761±3447	298±736	1886±1453	3545±2111
2012	Monsoon	8.9±5.1	56.8±40.6	2653±1011	68±75	976±473	1605±699
	post	19.6±14.0	97.4±82.5	4010±1965	118±142	1101±636	2446±1236

Tables 1 and 2 show that the seasonal variations of aerosol properties over Lahore and Jhelum respectively. Aerosol optical depth was maximum throughout the monsoon because the numbers of data points were very few, because of the prevalence of overcast conditions (cloudy in nature) during most of the days. In addition, the increase in AODs can occur because of hygroscopic growth of water soluble aerosols and transport of larger sized aerosols (dust and sea salt) during favorable wind conditions [24]. However, winter season shows much low levels of aerosol. optical depth as a result of monsoon rainfall and the post monsoon rainfall washes out most of the aerosol particles in the atmosphere.

Table 3 shows that during the two measurement years, there were contrasting monsoon seasons; with excessive rain in year 2011 than 2012 in both Lahore and Jhelum. In 2012 the rainfall was comparatively more in Jhelum than in Lahore, probably due to the location, as air masses owing uphill are more likely to form clouds and rain. Year 2011 exhibited the most rainfall in Lahore and in the whole of Punjab in general. The aerosol concentrations and the subsequent optical coefficients in the pre-monsoon season were highest in 2011 and 2012 (Table 1).

The average aerosol concentrations and optical coefficients during monsoon were decreased by about 40–75% compared to the pre-monsoon average concentrations at both stations, having a linear relationship with the total rainfall of the yearly monsoon season. The most effective decrease of the aerosol concentrations were observed during 2011 in Jhelum.

Table 3. Rainfall and Temperature data for Lahore and Jhelum for years 2011 and 2012.

		Month	Jan	Feb	Mar	Apr	May	Jun	Jul	Aug	Sep	Oct	Nov	Dec
2011	Lahore	Rainfall mm	18	234	423	526	42	167	342.32	635	1,576.80	6	13	11
		Record high °C	19	25	37	42	46	45	41	39	38	35	28	20
		Record low °C	3	9	11	15	24	20	20	25	23	16	14	2
	Jhelum	Rainfall mm	22	40	43	36	52	67	326	398	65	18	11	3
		Record high °C	17	20	33	38	40	42	41	39	38	35	28	20
		Record low °C	3	9	11	15	24	20	20	25	23	16	14	2
2012	Lahore	Rainfall mm	23	28.6	41.2	19.7	22.4	36	202	164	61.1	12	4.2	13.9
		Record high °C	27	30	37.2	44	47.4	47	45	41	40.6	39	34.4	28.1
		Record low °C	−1.1	1	5	10.6	14	18	20	19	16.7	11	1.7	0.6
	Jhelum	Rainfall (mm)	34	50	60	36	32	52	237	221	78	12	10	30
		Average high °C	20	22	27	33	38	40	36	34	35	33	28	21
		Average low °C	5	8	12	18	22	26	26	25	23	17	10	6

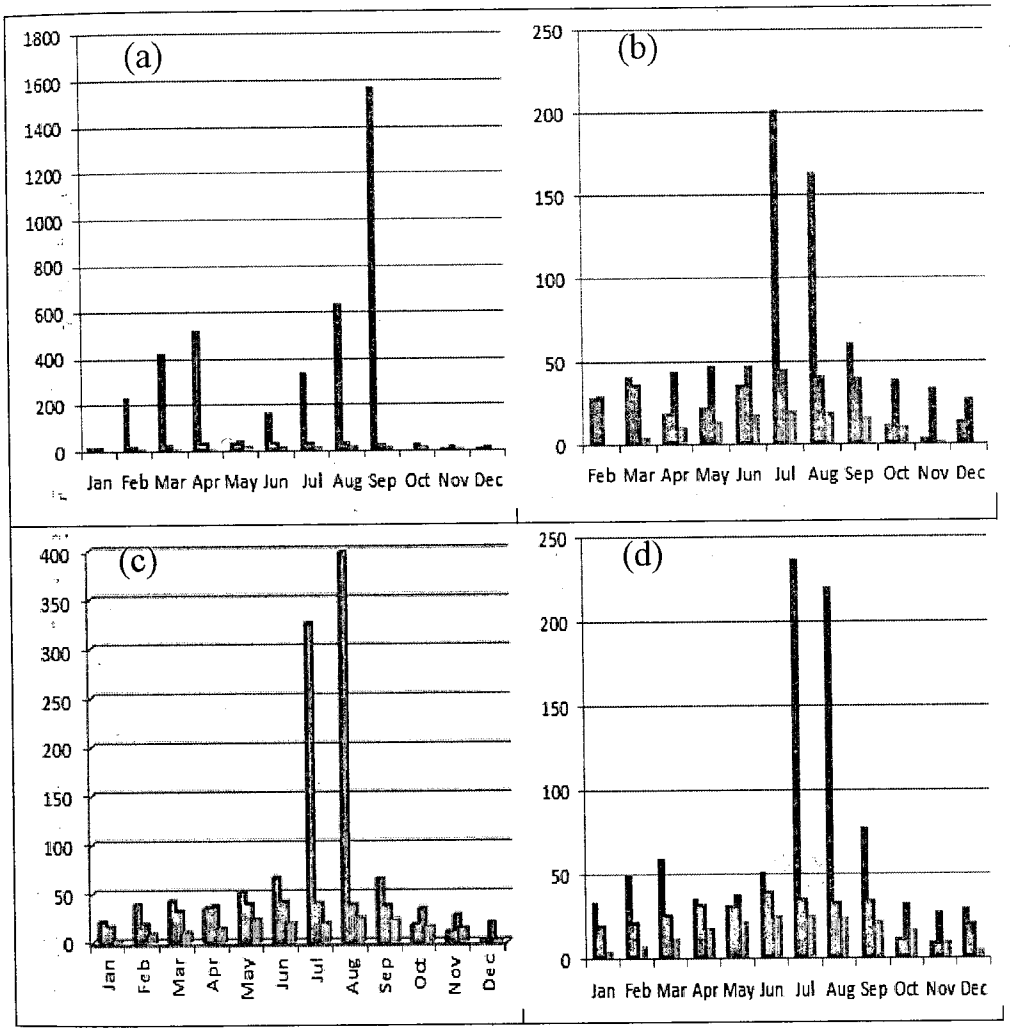

Fig. 2. Graphical representation of Rainfall and Temperature data for (a) Lahore 2011 (b) Lahore 2012 (c) Jhelum 2011 (d) Jhelum 2012

During 2011, the rain amounts were the highest of the study period in Lahore. During the post-monsoon season, concentrations rose again. In Lahore, the post monsoon averages were higher than the pre-monsoon averages. In Jhelum, however, the post monsoon averages were lower than the pre-monsoon averages. This behavior can be explained by the lower boundary layer height in the post-monsoon season [28].

The optical properties generally followed the seasonal behavior of concentration levels decreasing between 40–75% from the pre-monsoon average during monsoon (Table 1). In Jehlum the scattering coefficient decreased, on average, less than the absorption coefficient, mostly due to episodic peak concentrations

during the monsoon season. Light scattering is more effective, the bigger the particles are. So, again the increased light scattering can be related to mineral dust which was occasionally present during the break spells of the monsoon. The more effective decrease of the absorption coefficient indicates an efficient removal of absorbing aerosols in Jhelum. In Lahore, scattering coefficient showed occasional high concentrations, especially during 2012. In contrast to Jehlum, absorption coefficient in Lahore did not decrease very efficiently in the monsoon season. This can be explained by two reasons: first, the accumulation mode with the related absorbing particles was less effectively decreased during the monsoon in Lahore, because of the missing activation removal mechanism. Second, Lahore is located closer to pronounced anthropogenic combustion sources. This can be observed by the occasionally high absorption coefficients. During post-monsoon, a clear difference can be seen at the two stations – at Jhelum, both the absorption and scattering coefficient decreased compared to pre-monsoon, while in Lahore a substantial increase was observed. As mentioned before, this is related to the boundary layer evolution, as most of the pollution was confined below the altitude of Jhelum.

It was observed that the minimum monthly aerosol index was in November and maximum was in May for the year 2011. For 2012, maximum was found in May and minimum was found in January. The lowest seasonal averages of aerosol index for the year 2011 and 2012 were observed during the post monsoon and winter season respectively.

4. CONCLUSION

The present study has been concentrated on the trends of aerosol optical depth and rainfall over the two successive monsoon and post monsoon seasons for the years 2011 and 2012. We observed that at both stations, the average monsoon aerosol concentrations were smaller by 40–75% compared to the pre-monsoon average concentrations, decreasing with in-creasing total local rainfall during the monsoon season. Monsoon and post monsoon seasons Lahore in 2011 have more rainfall than the year 2012 because of aerosol optical depth has positive relationship with cloud optical depth, cloud effective radius, aerosol index, temperature and wind speed. As far as variations concerned, the aerosol index was more during 2012 and less in the active monsoon year. In case of cloud effective radius, it is directly related with rainfall and the study observed that during the post monsoon seasons, only cloud effective radius was found as upper limit. In addition, cloud optical depth also has direct association with cloud effective radius and rainfall in the study periods.

Acknowledgements: Measurements at Lahore and Jhelum stations were funded by the University Malaysia Sabah, Physics Department, Kota Kinabalu, Malaysia.

REFERENCES

1. J. Lelieveld, et al., Science, 291 (2001) 1031.
2. T. Nakajima, et al., J. Geophys. Res., 112 (2007) D24S91.
3. V. Ramanathan, J. Geophys. Res., 112 (2007) D22S21.
4. K. M. Lau and K.-M. Kim Geophys. Res. Lett., 33 (2006) L21810.
5. A. S. Ackerman, et al., Science, 288 (2000) 1042.
6. D. Rosenfeld, Science, 287 (2000) 1793.
7. V. Ramanathan, Science, 294 (2001) 2119.
8. A. Andreae, Science, 303 (2004) 1337.
9. Y. J. Kaufman, Proc. Nat. Acad. Sci. U.S.A., 102 (2005) 11207.
10. http://www.pakmet.com.pk/journal/july2003floods-sindh.htm
11. http://www.islamic-relief.com/wherewework/10-PK-1001-sindh-flood-relief-programme-2003-echo.aspx
12. http://pakistanweatherportal.com/2011/06/13/monsoon-2011-backlash-of-the-floods-history-of-pakistan-floods-in-detail/
13. http://www.dartmouth.edu/~floods/Archives/2007sum.htm
14. "Floods in Pakistan worse than tsunami, Haiti". gulfnews. Retrieved 2010-08-12.
15. http://www.reliefweb.int/rw/rwb.nsf/db900SID/LSGZ-89GD7W?OpenDocument
16. "Floods worsen, 270 killed: officials". *The Express Tribune*. 13 September 2011, Retrieved 13 September 2011.
17. http://dawn.com/2012/09/11/floods-triggered-by-downpour-wreak-widespread-devastation/.
18. C. E. Chung, V. Ramanathan, D. Kim and I. A. Podgorny, J. Geophys. Res., 110 (2005) 6356.
19. A. Chatterjee, C. Sarkar, A. Adak, U. Mukherjee, S. K. Ghosh, S. Raha, Aerosol Air Qual. Res., 13 (2013) 1133.
20. https://en.wikipedia.org/wiki/Lahore#cite_note-46
21. https://en.wikipedia.org/wiki/Jhelum
22. Y. J. Kaufman, D. Tanre and O. Boucher, Nature, 419 (2002) 215.
23. P. R. Salve, A. Maurya, D. S. Ramteke and S. R. Wate, Indian J. Environ. Prot., 26 (2006) 742.
24. S. Ramachandran, and R. Cherian, J. Geophys. Res., 113 (2008).

25. K. H. Kim, K. Sekiguchi, S. Kudo and K. Sakamoto, Japan. Aerosol Air Qual. Res., 11 (2010) 1.
26. D. Ganguly, A. Jayaraman and H. Gadhavi, J. Geophys. Res., 111 (2006).
27. S. Dey, S. N. Tripathi R. P. and Singh, J. Geophys. Res., 109 (2004).
28. T. Raatikainen, et al., Atmos. Chem. Phys. Discuss., 11, (2011) 11417.

PK ISSN 0022- 2941; CODEN JNSMAC
Vol. 53, (2013) PP 23-38

EFFECT OF LASER FLUENCE AND SUBSTRATE TEMPERATURE ON THE GROWTH OF SUPERCONDUCTING THIN FILMS PREPARED BY PULSED LASER DEPOSITION TECHNIQUE

M. F. SHAHZAD, S. BASHIR* AND K. MAHMOOD

Centre for Advanced Studies in Physics, G.C. University Lahore. PAKISTAN
*E-mail address: shaziabashir@gcu.edu.pk

(Received: January 09, 2014)

ABSTRACT: Superconducting BiVPbSrCaCuO thin films were deposited on Si (4 0 0) substrate by using pulsed laser deposition technique. For this purpose, Nd: YAG laser (532 nm, 6 nsec) was employed. The effect of varying laser fluence ranging from 2 to 5 J/cm^2 and varying substrate temperature ranging from room temperature to 700 °C on the growth of thin films was investigated. For the identification of crystalline structure of deposited films XRD analysis was carried out. SEM and AFM analysis was performed to analyze the texture and surface morphology of grown films. XRD results reveal that all deposited films exhibit the crystalline growth of BiPbSrCaCuO along the preferred orientations of (0 2 8) and (2 2 2). It was observed that both the crystallinity along the preferred orientations of (0 2 8) and grain growth increases with the increasing laser fluence. Optimum value of laser fluence was found to be 4 J/cm^2 for the growth of good quality films at room temperature. The results reveal that the substrate temperature also plays a significant role for the growth of good surface structures and the crystallinity of films along the preferred orientations of (0 2 8). The optimum value of the substrate temperature was found to be 500 °C at the laser fluence of 3 J/cm^2 for the deposition of highly crystalline and good textured films.

Keywords: PLD, BiVPbSrCaCuO superconductor, laser fluence, substrate temperature, thin film, crystalline structure, morphology.

1. INTRODUCTION

The synthesizing novel thin film by Pulsed Laser Deposition (PLD) is important area of current research. PLD offers the fastest route to prototyping any thin-film coating. In fact, many multicomponent materials produced with PLD promise valuable applications. It is a versatile technique for the fabrication of high quality superconducting thin films [1-3]. Several aspects of PLD are beneficial. It produces a highly forward-directed and confined plume of materials, which can be deposited with less contamination than the unconfined plasma in a sputter process. In addition, PLD is incredibly precise. It can deposit a film of YBCO that is one unit cell (1.2 nm) thick and experiments show that a single unit cell of YBCO is a superconductor. The growth of BiVPbSrCaCuO thin films is a field of great interest for superconducting device applications such as superconducting quantum interference devices (SQUID), microwave devices, generators, second generation superconducting devices and motors that operate at 77K [4-6].

The laser assisted deposition processes of thin films depends upon various laser parameters such as laser fluence, pulse width, deposition time or number of

shots. The other important deposition parameters which can significantly affect the quality, structure and morphological properties of the deposited thin films are nature and pressure of ambient gas, target to substrate distance and growth temperature. The effect of substrate temperature and oxygen pressure on the growth of superconducting thin films has been investigated by many research groups [7-9]. It is reported that the substrate temperature during deposition directly influences the crystal structure, morphology and orientation of grains [10-12]. However, a few works is reported in which the effect of laser fluence on the crystallinity, quality and compactness of superconducting films is addressed [13,14].

In this work superconducting thin films of BiVPbSrCaCuO are deposited on the silicon substrate by using pulsed laser deposition (PLD) technique. The motivation behind this work is to investigate the effect of laser fluence and substrate temperature on the growth of deposited films. The purpose was to investigate the optimum value of laser fluence and substrate temperature, where thin films of good quality, texture and improved crystallinity can be grown. Phase and crystallinity of deposited films were identified using X-ray diffraction (XRD) analysis. In order to correlate the structural characterization with the development of surface texture Atomic Force Microscope (AFM) and Scanning Electron Microscope (SEM) are employed.

2. EXPERIMENTAL PROCEDURE

Superconducting BiVPbSrCaCuO thin films were deposited on Si (4 0 0) substrate by pulsed laser deposition (PLD) technique. The experiment was performed by employing the Nd: YAG pulsed laser with the second harmonic of wavelength 532 nm, the maximum pulse energy of 600 mJ and a repetition rate of 10 Hz. The circular shaped superconducting discs of diameter 15 mm and of thickness 10 mm with stoichiometric ratios of Bi:V:Pb:Sr:Ca:Cu:O =1.5:0.1:0.4:2:2:3:8 were used as a target. The experiment was performed in Ultra High Vacuum (UHV) chamber which was evacuated to a base pressure of 10^{-9} Torr with the help of turbo molecular pump in conjunction with rotary pump. The beam was focused through a 50 cm focal length lens on the substrate distance was 5 cm and it was kept constant throughout the experiment. The target was placed on a rotating system to ensure uniform ablation. The schematic of experimental set-up is displayed in figure 1.The deposition was carried out in oxygen environment at a fixed pressure of 85 mTorr. Two sets of films were grown: (1) The Growth temperature was kept constant i.e. room temperature and films were grown at various laser fluences of (a) 2 J/cm^2 (b) 3 J/cm^2 (c) 4 J/cm^2

and (d) 5 J/cm^2,(2) Laser fluence was kept constant i.e. 3J/cm^2 and films were grown at various substrate temperatures of (a) Room temperature (b) 200 °C (c) 500 °C and (d)700 °C . The composition and crystallographic structure of the thin films was investigated using Xpert Pro (MPD) X-ray Diffractometer (XRD). Surface roughness and topography was measured using Atomic Force Microscope (AFM) Shimadzu (SMM-9500J3). The surface morphologies of deposited thin films were investigated by Scanning Electron Microscope (SEM) (Joel JM6480).

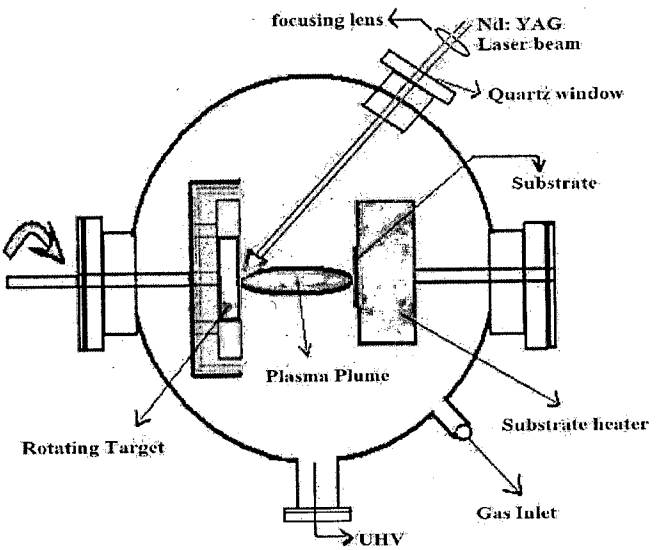

Fig. 1: The schematic of the experimental set-up for pulsed-laser deposition of superconducting (BiVPbSrCaCuO) thin films.

3. RESULTS AND DISCUSSION

3.1. XRD ANALYSIS

In order to investigate the effect of laser fluence and substrate temperature on the phase and crystallinity of deposited films, XRD analysis was performed.

(a) The Effect of Laser Fluence

The XRD patterns of (a) undeposited and deposited BiVPbSrCaCuO superconducting thin films on Si (4 0 0) substrate for various laser fluences of (b) 2 J/cm^2 , (c) 3 J/cm^2 , (d) 4 J/cm^2 , (e) 5 J/cm^2 are presented in figure 2. It is clearly seen that BiVPbSrCaCuO thin films are deposited with (0 2 8) and (2 2 2) preferred orientation and are therefore polycrystalline in nature. No such phases

are observed for undeposited sample. One peak identified at 2θ=69.28° corresponds to a substrate single crystal Si (4 0 0). This loss of vanadium in the identified peaks is due to the scattering of vanadium elements by the oxygen pressure [15].

As the laser fluence increases from 2 J/cm^2 to 3 J/cm^2 and to 4 J/cm^2 the intensity of the peak corresponding to plane (0 2 8) increases as depicted by figure 2 (b-d). By increasing the laser fluence the kinetic energy of adatoms BiVPbSrCaCuO increases.

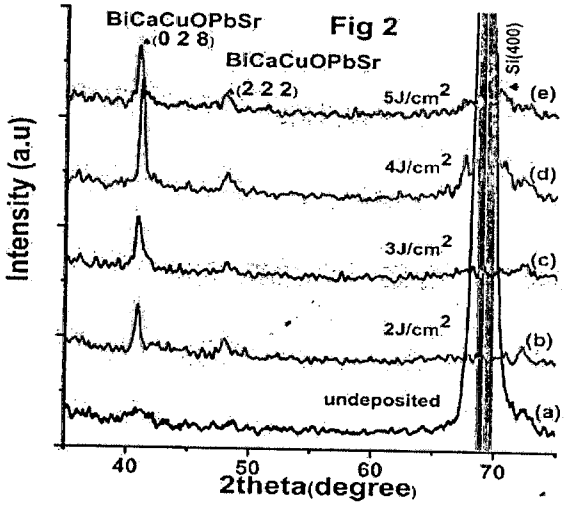

Fig. 2: XRD patterns of (a) Undeposited and deposited superconducting films on Si (4 0 0) substrate for various laser fluences of (b) 2 J/cm^2, (c) 3 J/cm^2, (d) 4 J/cm^2 and (e) 5 J/cm^2.

These adatoms with high K.E accommodate themselves at appropriate lattice sites of the substrate and hence resulting into the improvement of the crystalline quality of the film with preferred orientation of (0 2 8). As fluence is further increased to value of 5 J/cm^2 as depicted in figure 1(e), peak intensity decreases. This decrease is attributed to the degradation of crystalline structure with preferred orientation of (0 2 8). As the fluence increase, the K.E of the ejected species increases. If the fluence is very high; aggregation and fragmentation takes place [16].

If the energy of ejected species is sufficiently high enough, then the mobility of these adatoms will not allow them to accommodate at appropriate lattice site. In this case the crystalline structure degrades and corresponding peak intensity of that preferred orientation also decreases.

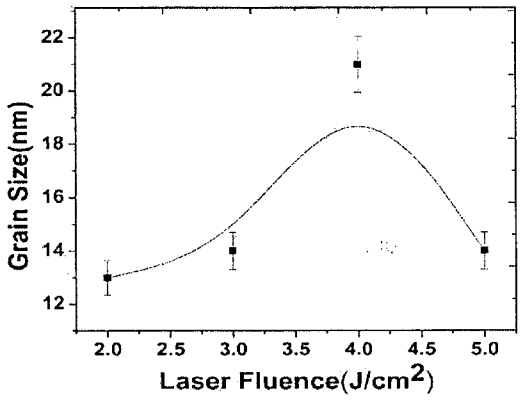

Fig. 3: The grain size of superconducting thin film corresponding to (0 2 8) diffraction peak for various laser fluences.

The average crystalline size D was calculated from the full-width at half maximum (FWHM) using the Scherer formula [17].

$$D = \frac{0.94\lambda}{\beta \cos(\theta)} \quad (1)$$

where λ is the x-ray wavelength of 1.542 Å, θ is the Bragg's diffraction angle, and β is the full width at half maximum (FWHM) of the peak corresponding to plane (0 2 8). The average grain size of the deposited films comes out to be 13 nm, 14 nm, 21 nm, and 14 nm for laser fluence of 2, 3, 4 and 5 J/cm^2 respectively which is plotted in figure 3. It indicates that the grain size of the grown films increases with increasing laser fluence up to 4 J/cm^2. As fluence is further increased to value of 5 J/cm^2, grain size decreases. The minimum value of FWHM is obtained at 4 J/cm^2. The highest value of peak intensity, and crystalline size and minimum value of FWHM of BiVPbSrCaCuO for (0 2 8) implies that 4J/cm^2 is the optimum value of laser fluence for the growth of highly crystalline films.

(b) The Effect of Substrate Temperature

The XRD patterns of (a) undeposited and deposited BiVPbSrCaCuO superconducting thin films on Si (4 0 0) substrate for various growth temperatures of (b) RT, (c) 200 °C, (d) 500 °C, and (e) 700 °C at a fluence of 3 J/cm^2 are exhibited in Fig. 4. It is clearly seen that BiVPbSrCaCuO thin films are deposited with (0 2 8) and (2 2 2) preferred orientation and therefore polycrystalline in nature. No such phases are observed for undeposited sample. Again significantly intense peak observed at 2θ = 69.28° is representing the Si substrate. As the

growth temperature increases from a room temperature, 200°C and to 500 °C as illustrated in figure 4(b-c). It implies that increasing temperature favors the preferential growth along (0 2 8) plane. As the temperature further increases to value of 700°C as depicted in figure 4(e), peak intensity decreases. This decrease is attributed to the degradation of crystalline structure with preferred orientation of (0 2 8).

During the deposition; the atomic kinetic energy is mainly determined by the substrate temperature at fixed laser fluence. As the growth temperature increases, the mobility of the adatoms increases and these atoms have high diffusion activation energy to occupy appropriate lattice site in the crystal. In other words these atoms look for the lowest energy sites and constitute the low energy structure [18,19] .The diffusion of atoms at lower surface energy causes preferable grain-growth at high substrate temperature. Then the growth orientation develops into the one crystallographic direction of the low surface energy as displayed in Fig. 4. However if the substrate temperature is too high then re-evaporation, resputtering of the deposited particulates occurs. This leads to degradation of crystalline structure and correspondingly the peak intensity of that preferred orientation also decreases.

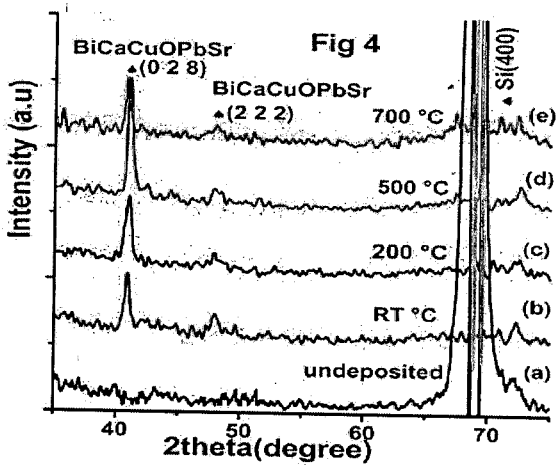

Fig. 4: XRD patterns of (a) Undeposited and deposited superconducting thin films on Si(4 0 0) substrate for various growth temperatures of (b) RT_1, (c) 200 °C, (d) 500°C, and (e) 700 °C for fixed fluence of 3 J/cm^2.

The average grain size evaluated from Scherer formula [9] of deposited films comes out to be 14, 17, 21 and 17 nm for growth temperature of RT, 200, 500 and 700 °C respectively and is plotted in Fig. 5. This illustrates that the grain size of the grown films increases with increasing growth temperature up to a value of 500°C. As the temperature further increases to value of 700°C, grain size

decreases. The highest value of peak intensity, and crystallite size and minimum value of FWHM of BiVPbSrCaCuO for (0 2 8) plane implies that 500°C is the optimum value of temperature for the growth of highly crystalline films.

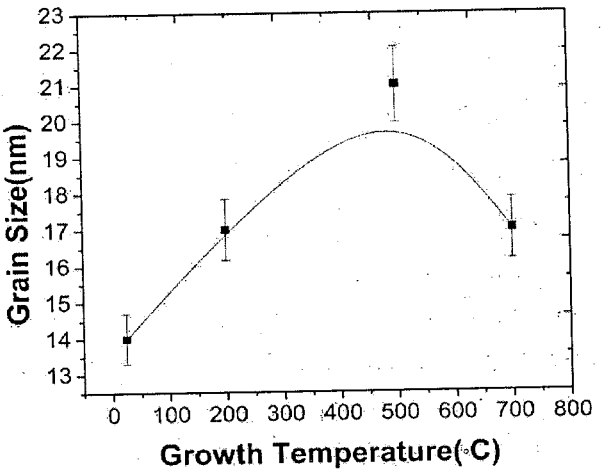

Fig. 5: The grain size of superconducting thin film corresponding to (0 2 8) diffraction peak for various growth temperatures.

3.2. AFM ANALYSIS

In order to investigate the effect of laser fluence and substrate temperature on the surface topography and roughness of deposited films, AFM analysis was performed.

(a) The Effect of Laser fluence

Figure 6 shows three-dimensional AFM surface topographical images (scan area 5 μm x 5 μm) of grown BiVPbSrCaCuO thin films on Si substrate, for four various laser fluences of (a) 2 J/cm^2 (b) 3 J/cm^2 (c) 4 J/cm^2 and (d) 5 J/cm^2. All films were deposited at room temperature. The appearance of an uneven surface with protrusions and grains of an unequal size is clearly seen in figure 6 (a) for laser fluence of 2 J/cm^2. When the laser fluence is increased up to a range of 3 J/cm^2, the uniformity of the film and size of grains grown on the substrate surface increases as shown in figure 6 (b). Further increase in the fluence up to a range of 4 J/cm^2 leads to uniform grain growth as displayed in figure 6 (c). The surface becomes highly uneven with further increase of fluence up to range of 5 J/cm^2. These results are further confirmed by the Root Mean Square (RMS) values of surface roughness which are listed in Table 1. The root-mean-square (RMS) for 2 J/cm^2 comes out to be 63 nm. It decreases to value of 53 nm with the

increasing fluence up to a value of 3 J/cm^2. Further increase in the fluence makes the film more uniform and RMS values come out to be 51 nm at fluence of 4 J/cm^2. The surface roughness again increases to 78 nm with further increase of laser fluence of 5 J/cm^2. Hence the optimum value of laser fluence was 4 J/cm^2 where lowest surface roughness was observed. These results are in compatible with XRD results in which the maximum crystallinity is observed for a fluence of 4 J/cm^2.

In the pulsed laser deposition process, the laser fluence is the controlling parameter for the flight speed of the plasma and the kinetic energy of ejected species. With the increase of laser fluence the BiVPbSrCaCuO atoms obtained larger kinetic energy and hit the silicon surface forcefully. The energy provided by this hitting process may have accelerated the surface diffusion process and favored the formation of uniform aggregated structures and grains [16] as shown in figure 6 (c). Moreover; at high laser fluence of 5J/cm^2, the BiVPbSrCaCuO atoms were easily more aggregated with the high K.E, and some of them are fragmented after resputtering which resulted in to the higher surface roughness as shown in figure 6 (d). This resulted in poor crystal quality which can be confirmed from XRD measurements as shown in figure 2. It is evident from figure 2 that at the highest laser fluence of 5 J/cm^2, the FWHM increases and intensity of the (0 2 8) diffraction peak decreases.

It may be possible that at higher laser fluence some atoms with too high K.E could not reach at appropriate lattice sites and some cause resputtering which eventually resulted in poor crystal quality.

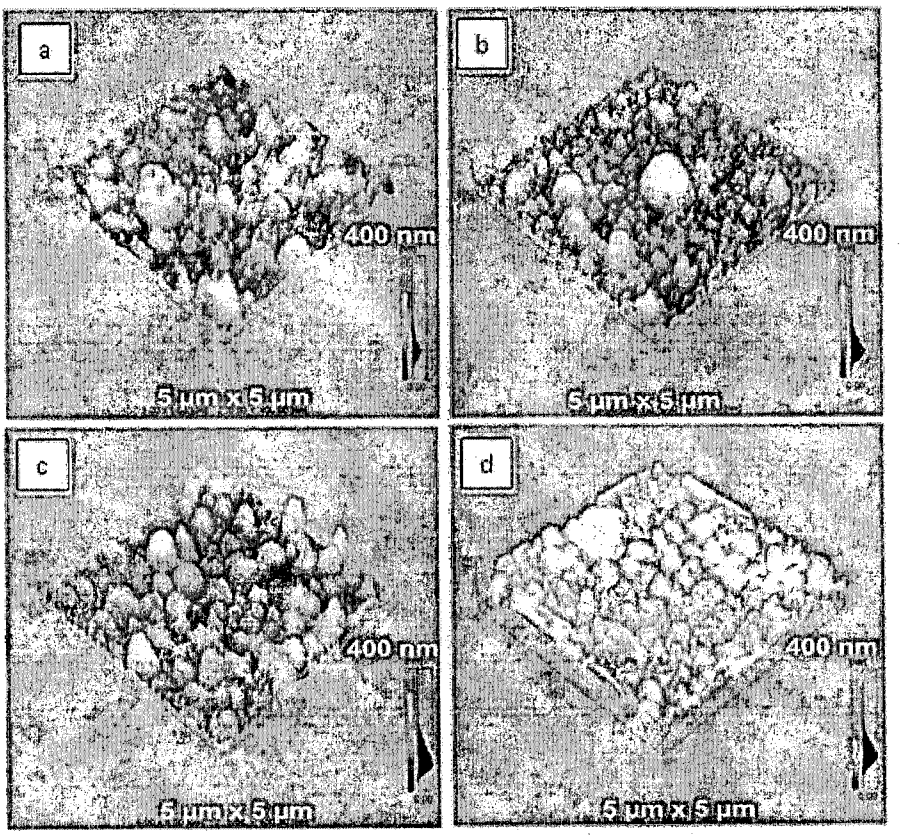

Fig. 6: AFM images for scan area of (5 µm x 5 µm) of the deposited superconducting thin films for various laser fluences of (a) 2 J/cm^2 (b) 3 J/cm^2 (c) 4 J/cm^2 and (d) 5 J/cm^2.

(b) The Effect of Substrate Temperature

Figure 7: displays three-dimensional AFM images of the BiVPbSrCaCuO thin films deposited at different substrate temperatures of (a) RT, (b) 200°C, (c) 500°C, and (d) 700°C at fixed fluence of 3 J/cm^2. The scanning area is 5 µm x 5 µm. The root-mean-square (RMS) values of surface roughness for deposited films are listed in table 2. Films deposited at different substrate temperatures showed different surface roughness and textures. The deposited films showed, 3D columnar growth of grains [10] completely covering the whole film surface as shown in figure 7. At room temperature the surface roughness of the deposited thin film was found to be 53 nm. The surface roughness of thin films initially increases with increasing temperature and becomes 57 nm when substrate temperature is 200°C. The density of grown grains and particulates significantly increases at this temperature. Further increase in temperature up to a value of 500°C causes reduction in the roughness and its value comes out be lowest i.e.

52 nm . The size of grown structures increases and density of grains decreases. Further increase in substrate temperature up to a range of 700°C, the surface roughness again increases to a value of 66 nm resulting in poor quality and non-uniform texture of film.

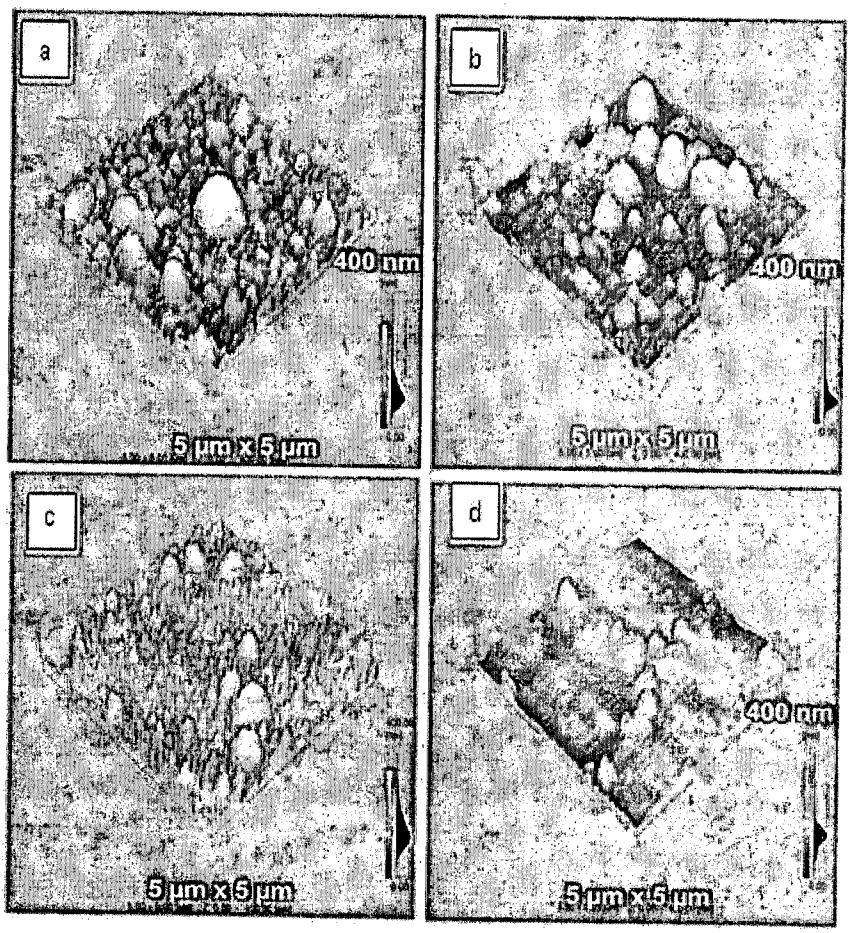

Fig. 7: AFM images for scan area of (5 μm x 5 μm) of the deposited superconducting thin films for laser fluence of 3J/cm^2 deposited at various substrate temperatures of (a) RT (b) 200° C (c) 500° C and (d) 700° C.

When substrate temperature increases, the mobility of target atoms increases. The fast diffusion of highly mobile ions contributes significantly for their easy arrival at equilibrium position. Therefore initially increasing substrate temperature up to a value of 500°C, better film growth along with perfect crystalline structure is highly probable. It is also confirmed by XRD results (figure 4). Further increase in temperature results in to poor film quality. This is due to re- evaporation of particles at higher substrate temperature. This can be confirmed in XRD

measurements in figure 4, where the diffraction peak intensity decreases and the FWHM increases when the substrate temperature was too high to a value of 700°C.

Table 1: The RMS values of the surface roughness of the deposited superconducting thin films for various laser fluencies.

Laser fluence (J/cm^2)	2	3	4	5
RMS values of Surface roughness (nm)	63	53	51	78

Table 2: The RMS values of the surface roughness of the deposited superconducting thin films with laser fluence of 3J/cm^2 deposited at various substrate temperatures.

Substrate temperature (°C)	RT	200	500	700
RMS values of Surface roughness (nm)	53	57	52	66

3.3. SEM ANALYSIS

In order to investigate the effect of laser fluence and substrate temperature on the surface morphology of deposited superconducting thin films, SEM analysis was performed.

(a) The Effect of Laser Fluence

Figures 8(a-d) reveals the SEM images of grown BiVPbSrCaCuO thin films on Si substrate for four different laser fluences of (a) 2 J/cm^2, (b) 3 J/cm^2, (c) 4 J/cm^2 and (c) 5 J/cm^2.

The lowest particle density of grown film is seen in figure 8(a), which corresponds to lowest laser fluence. The increasing laser fluence (3 J/cm^2) leads to increased particle density, but film texture is not improved as can be clearly seen in figure 8 (b). When the fluence is increased upto a value of 4J/cm^2 very high particle density with significantly improved films texture is observed which is exhibited in figure 8(c).

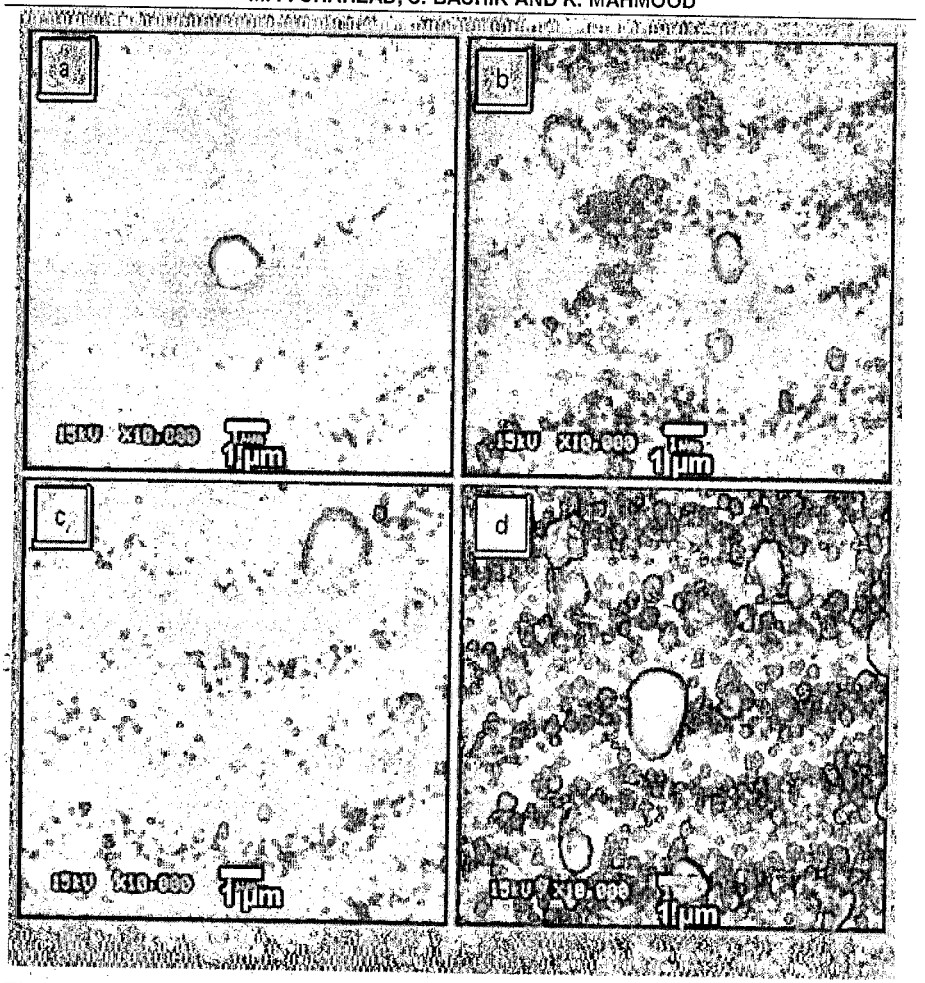

Fig. 8: SEM images of the deposited superconducting thin films for various laser fluences of (a) 2 J/cm^2 (b) 3 J/cm^2 (c) 4 J/cm^2, and (d) 5 J/cm^2.

This fluence is therefore can be considered as an optimum fluence value for growth of better quality films and is in agreement with XRD measurements. However, as the laser fluence is further increased up to maximum value of 5 J/cm^2, both the density of particles and grain size increases. But the uniform film texture is destroyed as is seen in figure 8 (d). The BiVPbSrCaCuO atoms easily get aggregated with the higher K.E. at higher fluences. This results into resupttering and destruction of uniform film texture [20]. This further leads to poor crystal quality which is confirmed in XRD measurements as has been explained from figure 2.

(b) The Effect of Substrate Temperature

The effect of various growth temperatures of (a) RT, (b) 200°C, (c) 500°C, and (d) 700°C at fixed fluence of 3J/cm^2 on the texture growth BiVPbSrCaCuO thin films

are revealed by SEM images of figure 9. It is evident that density and grain size of the particles increases with increasing the substrate temperature from RT-500°C (figure a-c). Beyond 500 °C (figure 9 d) size and density of particles again starts decreasing. This is in agreement with XRD analysis. A possible explanation is that as substrate temperature increases, the mobility and diffusion of deposited atoms increases. This supports crystallization which will cause enhanced coalescence and nucleation of grown film. In this way the texture and quality film is improved as is represented by figure 9(a-c). When the substrate temperature is too high (say 700°C or higher), the adatoms with too high kinetic energy collide with each other and re-evaporate quickly. This dislocation of the mass in the thin film degrades the film quality as is demonstrated in Fig.9 (d).

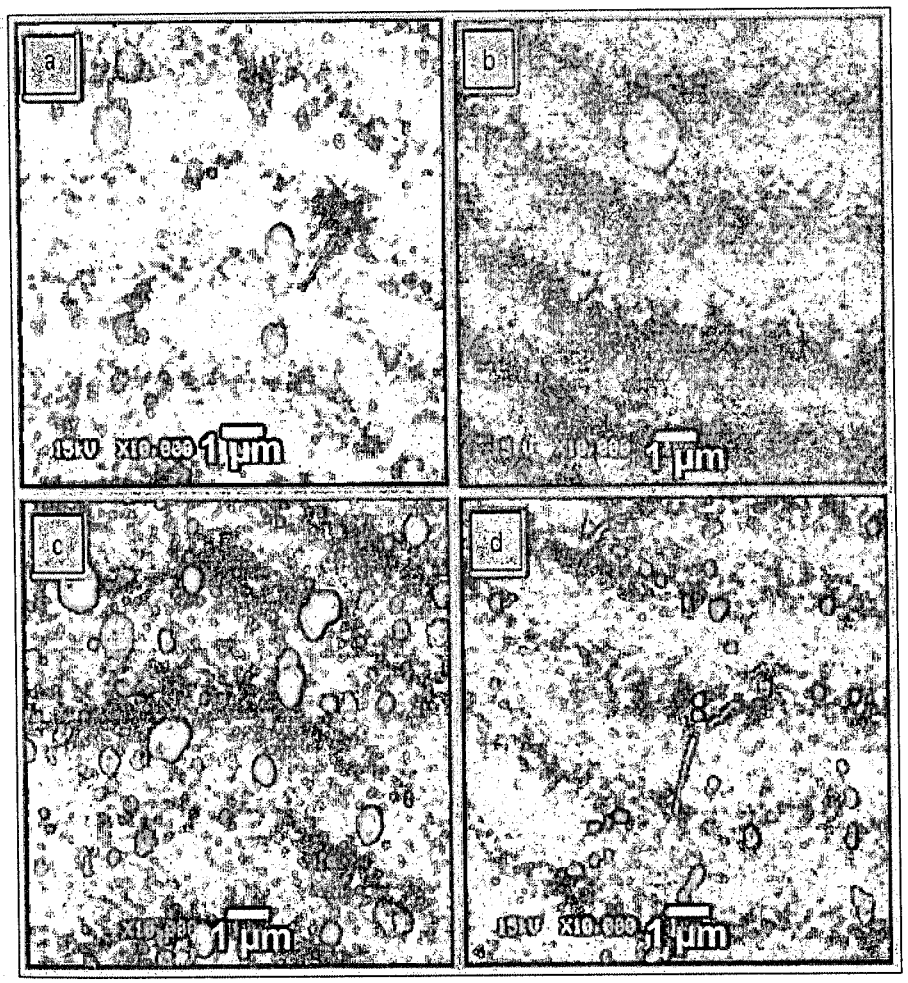

Fig. 9: SEM images of the superconducting thin films deposited for a laser fluence of 3 J/cm^2 at substrate temperature of (a) RT (b) 200 °C (c) 500 °C (d) 700 °C.

4. CONCLUSIONS

The optimum conditions for the growth of pulsed laser deposited BiVPbSrCaCuO superconducting thin films have been determined. The structure, surface topography and texture are extremely sensitive to laser fluence and substrate temperature. The effect of laser fluence and substrate temperature on the microstructure, surface roughness and morphology of the superconducting thin films has been investigated by means of X-ray diffraction (XRD), atomic force microscope (AFM) and scanning electron microscope (SEM). It is found that superconducting thin films deposited with a laser fluence of 4 J/cm^2 has the strongest peak with preferred orientation of (0 2 8) with minimum FWHM, implying the best crystal quality. It is also found that film deposited with a laser fluence of 4J/cm^2 has the minimum RMS value of 51 nm as revealed by AFM analysis. Furthermore SEM results reveal that by increasing laser fluence the density of the particles increases along with improvement of film texture. These results show that optimum value for the formation of superconducting thin film is 4 J/cm^2.

It is revealed that substrate temperature also plays a significant role in determining the properties of BiVPbSrCaCuO superconducting thin films. The XRD and SEM results show that structure and crystalline quality of thin films increased from 200 °C to 500 °C but was degraded when temperature reached at 700 °C. It is found that film deposited at a substrate temperature of 500 °C had the strongest peak with preferred orientation of (0 2 8) with minimum FWHM, implying the best crystal quality. Furthermore minimum RMS value of 52 nm was obtained from AFM results. Hence the optimum value of temperature for the deposited thin films is found to be 500 °C.

REFERENCES

1. J. C. D. Vero, J. L. F. Gabayno, W. O. Garcia and R. V. Sarmago, Physica C, 470 (2010) 149.
2. Y. Ichino, Y. Yoshida, T. Yoshimura, Y. Takai, M. Yoshizumi, T. Izumi and Y. Shiohara, Physica C, 470 (2010) S1003.
3. A. H. Farha, A. E. Oguz, Y. Ufuktepe and H. E. E. Ali, Mat. Chem. & Phys., 132 (2012) 667.
4. S. Saini, M.Takamura, M. Mukaida and S. J. Kim, Current Appl. Phys., 11 (2011) 79.

5. J. C. D. Vero, G. R. S. Blanca, J. R. Vitug, W. O. Garcia and R. V. Sarmago, Physica C, 471 (2011) 378.
6. T. Haugan, P. N. Barnes, L. Brunke, I. Maartense and J. Murphy, Physica C, 397 (2003) 47.
7. R. Rossler, J. D. Pedarnig and C. Jooss, Physica C, 361 (2001) 13.
8. S. Duhalde, A. Lamagna, M. Villafuerte, A. Schwartzman, L. Correra and G. Quintana, Thin Appl. Surf. Sci., 127 (1998) 520.
9. K. Kikunaga, T. Yamamoto, Y. Tanaka, N. Kikuchi, K. Tokiwa, T. Watanabe and N. Terada, Physica C, 470 (2010) 1916.
10. S. Y. Yang, B.Y. Man, M. Liu, C. S. Chen, X. G. Gao, C. C. Wang and B. Hu, Appl. Surf. Sci., 257 (2011) 3856.
11. O. M. Ntwaeaborwa, P. D. Nsimama, J. T.Abiade, E. Coetsee and H. C. Swart, Physica B, 404 (2009) 4436.
12. S. Senthilarasu, R. Sathyamoorthy and S. K. Kulkarni, Materials Science and Engineering B, 122 (2005) 100.
13. S. G. Jung, E. M. Choi, N. H. Lee, Y. S. Kwon, W. N. Kang, D. H. Kim, M. H. Jung, S. I. Lee and L. Sun, Physica C, 470 (2010) S511.
14. M. Branescu, A. Vailionis, J. Huh, A. Moldovan and G. Socol, Appl. Surf. Sci., 253 (2007) 8179.
15. M. C. Foote, R. P. Vasquez, B. B. Jones, B. D. Hunt and J. B. Barrier, J. Elect. Mat., 23 (1994) 849.
16. B. Y. Man, S. C. Xu, C. Yang, M. Liu, S. Z. Jiang, Y. Y. Ma, C. S. Chen, A. H. Liu, X. G. Gao, C. C. Wang and B. Hu, Appl. Surf. Sci., 257 (2011) 6321.
17. A. Guinier, "X-ray diffraction in crystals, imperfect crystals, and amorphous bodies", San Francisco, W. H. Freeman, (1963), New York.
18. M. Liu, X. Q. Wei, Z. G. Zhang, G. Sun, C. S. Chen, C. S. Xue, H. Z. Zhuang and B.Y. Man, Appl. Surf. Sci., 252 (2006) 432.
19. K. S. Kim, H. W. Kim and C. M. Lee, Mat. Sci. Eng. B, 98 (2003) 135.
20. L. Fang and M. Shen, J. Cryst. Growth, 310 (2008) 3470.

PK ISSN 0022- 2941; CODEN JNSMAC
Vol. 53, (2013) PP 39-78

UIR MATRIX ELEMENTS 0F FINITE TRANSFORMATIONS OF SO(2,1) DECOMPOSED ACCORDING TO THE SUBGROUP SO(1,1)

A. SYED

Department of mathematics, BUITMS, Quetta, Pakistan
E-mail address: ansaruddinsyed@gmail.com

(Received: May 29, 2013)

ABSTRACT: Matrix elements of finite transformations of SO (2, 1) in representations of principle series of integral type, decomposed according to the subgroup SO (1, 1), have been obtained by Mukunda by using the method of differential equations satisfied by these elements. However, he is able to do this only for rotations of the type

$I_2(\xi)\, I_1(\zeta)\, I_2(\xi')$ and $I_2(\xi)\, r_0(\theta)\, I_2(\xi')$.

Although, as pointed out by himself, there do exist large number of elements SO(2, 1) which cannot be put in this form. Using a completely different method based, after choosing p=2, on the multiplier representation of SO(p, 1) decomposed according to the subgroup SO(p – 1, 1), constructed by Boyer and Ardalan, we in the present paper, compute the above matrix elements for arbitrary transformations of SO(2, 1); for the purpose, we have to transform a parameterization of arbitrary elements of SL(2, R) given by Vilenkin, into one for arbitrary element of SO(2, 1) by using an appropriate 2-1 onto homomorphism SL(2, R) → SO(2, 1). We also check that our results, for the cases considered by Mukunda, agree with his results.

Keywords: Unitary irreducible representations (UIR), SO(2, 1), SO(1, 1)
Subject Classification: PACS No. 02.20 Qs

1. INTRODUCTION

The problem of determination of UIR matrix elements of finite group transformations of compact and non-compact rotation groups, has a pretty long history. It was originated by Wigner [1] in 1930's when he obtained his famous d-functions which are simply the matrix elements of finite rotations of the ordinary rotation group SO(3). The next step was taken by Bargmann [2] in 1947, when he obtained the matrix elements of finite transformations of the Lorentz groups SO(2, 1) and SO(3, 1). Ever since early sixties, there have been a large number of papers (for details see [3]), not only concerning these simple groups but also the more general ones SO(n), SO(n , 1) and SO(n, 2).

An important aspect of these studies concerns the selection of basis for the carrier space of the representation. Generally, the choice is such that its elements are eigenvectors of not only the Casimir operators of the group itself but also of the Casimir operators of some maximal subgroup of it. We express this situation

by saying that the representation has been *decomposed* or *reduced* according to the particular maximal subgroup. This matter becomes specially important in the case of non-compact groups as here, we have compact as well as non-compact maximal subgroups. The problem is obviously simpler for decomposition according to compact subgroups, so that most of the papers, specially the earlier ones, deal with this case only. For decomposition according to the non-compact subgroups, some progress was made in the seventies and eighties for SO(2, 1) (see [4]) for the decomposition

$SO(2, 1) \supset SO(1, 1)$

and for the most degenerate representations (in which all Casimir operators except one, are zero) of SO(n, 1) and SO(n,2) (see [5]) , for the decompositions

$SO(n, 1) \supset SO(n-1, 1)$,

$SO(n, 2) \supset SO(n, 1)$

But, for example, no expressions for matrix elements of SO(3, 1) for the decomposition

$SO(3, 1) \supset SO(2, 1)$

yet exist for the non-degenerate representations.

As mentioned above, Mukund [4] has computed the UIR matrix elements of finite transformations of SO(2, 1) decomposed according to the subgroup SO(1, 1). However, he has done this only for the elements of SO(2,1) of the form

$I_2(\xi)\, I_1(\zeta)\, I_2(\xi')$ and $I_2(\xi)\, r_0(\theta)\, I_2(\xi')$,

and has pointed out that there exist a large number of other elements which cannot be put in this form. Our aim in the present paper is to extend these results of Mukunda by obtaining these matrix elements for ALL elements of SO(2, 1). However, we use a method totally different from that of Mukunda, although we do show that our results coincide with his results for the cases which he has dealt with. Our method depends on the work of Boyer and Ardalan [6] , who have set up a most degenerate representation of Principle series, of SO(p, 1) decomposed according to the subgroup SO(p – 1, 1), as a multiplier representation on the space of functions on the two sheeted hyperboloid in p dimension. As every representation of SO(2,1) is automatically most degenerate, we take over their representation with p=2; we then choose an appropriate basis in the carrier space and then use the parameterization of elements of SO(2,1) obtained by an appropriate homomorphism, from a parameterization of elements of SL(2, R) given by Vilenkin [7] , to calculate the matrix elements of arbitrary rotations of SO(2,1).

2. THE REPRESENTATION T^{σ}

Boyer and Ardalan [6] construct a multiplier representation $T^{\sigma 2}$, which we shall denote by just T^{σ}, of SO(2, 1) on the Hilbert space $L^2(H^{(1)})$ of square integrable functions on the two-sheeted hyperboloid

$H^{(1)} = \{ \eta \equiv \eta_{\mu} \eta^{\mu} \eta_{\mu} \equiv -\eta_1^2 + \eta_0^2 = 1 \};$

as $H^{(1)}$ is the union of two sheets

$H_{\pm}^{(1)} = \{\eta_{\mu}: \eta^{\mu} \eta_{\mu} \equiv -\eta_1^2 + \eta_0^2 = 1, \eta_0 > 0, <0 \}$,

$L^2(H^{(1)})$ breaks up as a direct sum of spaces of square integrable functions on $H_+^{(1)}$ and $H_-^{(1)}$

$L^2(H^{(1)}) = L^2(H_+^{(1)}) \oplus L^2(H_-^{(1)})$.

The inner product on $L^2(H_{\pm}^{(1)})$ is given by

$$(f_1, f_2) = \int_{H_{\pm}^{(1)}} d\Omega f_1^{\times}(\Omega) f_2(\Omega), \qquad (1)$$

where $d\Omega$ is the usual invariant measure on $H_{\pm}^{(1)}$. The action of the operator $T^{\sigma}(g)$, representing the element $g \varepsilon SO(2, 1)$, on the function

$f \varepsilon L^2(H^{(1)})$,

is given by (equation (2.3) of [6])

$$T^{\sigma}(g) f(\eta) = \left| (g^{-1})_2{}^{\nu} \eta_{\nu} + (g^{-1})_2{}^2 \right|^{\sigma} \times f\left(\frac{(g^{-1})_{\mu}{}^{\nu} \eta_{\nu} + (g^{-1})_{\mu}{}^2}{(g^{-1})_2{}^{\nu} + (g^{-1})_2{}^2} \right) \qquad (2)$$

Note that the in dices μ, υ, take on the values 0,1, only. When σ is given by

$\sigma = -\frac{1}{2} + i\rho$, ρ real, $\rho \geq 0$,

T^{σ} is found [6] to be a unitary irreducible representation of principle series of integral type.

3. PARAMETRIZATION OF GROUP ELEMENTS

As mentioned earlier, Mukunda [4] carries out his calculations only for those elements SO(2, 1) which can be put in the form

$I_2(\zeta) I_1(\upsilon) I_2(\zeta')$ or $I_2(\zeta) r_0(\mu) I_2(\zeta')$,

and then points out that elements of these forms do not exhaust the group. We therefore consider a parameterization which is valid for all elements of SO(2, 1). This is obtained from the work of Vilenkin [7] who shows that an arbitrary element of SL(2, R) , none of whose elements is zero, can be put in the form

$g = d_1(-e)^{\varepsilon_1} s^{\varepsilon_2} p d_2$

where ε_1 and ε_2 take the values 0 or 1, d_1, d_2 are diagonal matrices of the form

$$\begin{bmatrix} e^{-\phi} & 0 \\ 0 & e^{\phi} \end{bmatrix},$$

e is the 2×2 unit matrix,

$$s = \begin{bmatrix} 0 & 1 \\ -1 & 0 \end{bmatrix},$$

and p is a matrix of one of the following two types

a) $$p = \begin{bmatrix} ch\theta & sh\theta \\ sh\theta & ch\theta \end{bmatrix}, \quad -\infty < \theta < \infty,$$

b) $$p = \begin{bmatrix} \cos\theta & -\sin\theta \\ \sin\theta & \cos\theta \end{bmatrix}, \quad -\pi/4 < \theta < \pi/4,$$

while an element, one of whose matrix elements is zero, can be put in the form

$$g = d(-e)^{\varepsilon_1} s^{\varepsilon_2} p s^{\varepsilon_3},$$

where d, s, and e are as above, $\varepsilon_1, \varepsilon_2, \varepsilon_3$ take on the values 0 and 1, and p is a triangular matrix of the form

$$\begin{bmatrix} 1 & 0 \\ x & 1 \end{bmatrix}, \quad -\infty < x < \infty.$$

In order to transform this parameterization from SL(2, R) to SO(2, 1), we have to proceed in two steps; first, we transform it from SL(2, R) to SU(1, 1) and then from SU(1, 1) to SO(2, 1). For the purpose, we have to use the (slightly modified) isomorphism of SL(2, R) to SU(1, 1) given by Knapp [8] and the 2-1 homomorphism of SU(1, 1) onto SO(2, 1), given by Bargmann [2]. We now give the details of this transformation of parameterization from SL(2, R) to SO(2, 1).

Knapp [8] (p. 39) gives an isomorphism between SL(2, R) and SU(1, 1) by

$$\begin{bmatrix} 1 & i \\ i & 1 \end{bmatrix} SU(1,1) \begin{bmatrix} 1 & i \\ i & 1 \end{bmatrix}^{-1} = SL(2,R)$$

This gives, $$\begin{bmatrix} 1 & i \\ i & 1 \end{bmatrix}^{-1} SL(2,R) \begin{bmatrix} 1 & i \\ i & 1 \end{bmatrix} = SU(1,1).$$

We need a simple modification of this; as

$$\begin{bmatrix} 1 & 1 \\ 1 & -1 \end{bmatrix} SL(2,R) \begin{bmatrix} 1 & 1 \\ 1 & -1 \end{bmatrix}^{-1} = SL(2,R)$$

is obviously an isomorphism of SL(2,R) onto itself,

$$\begin{bmatrix}1 & i\\ i & 1\end{bmatrix}^{-1}\begin{bmatrix}1 & 1\\ 1 & -1\end{bmatrix}SL(2,R)\begin{bmatrix}1 & 1\\ 1 & -1\end{bmatrix}^{-1}\begin{bmatrix}1 & i\\ i & 1\end{bmatrix}=SU(1,1) \tag{3}$$

will also be an isomorphism between SL(2,R) and SU(1,1), and this is the one that we need.

Under (3), we check that

$$\begin{bmatrix}e^{\zeta/2} & 0\\ 0 & e^{-\zeta/2}\end{bmatrix}\leftrightarrow\begin{bmatrix}ch\zeta/2 & sh\zeta/2\\ sh\zeta/2 & ch\zeta/2\end{bmatrix},$$

$$\begin{bmatrix}ch\zeta/2 & sh\zeta/2\\ sh\zeta/2 & ch/2\end{bmatrix}\leftrightarrow\begin{bmatrix}ch/2 & ish\zeta/2\\ -ish\zeta/2 & ch\zeta/2\end{bmatrix},$$

$$\begin{bmatrix}\cos\theta/2 & \sin\theta/2\\ -\sin\theta/2 & \cos\theta/2\end{bmatrix}\leftrightarrow\begin{bmatrix}e^{-i\theta/2} & 0\\ 0 & e^{i\theta/2}\end{bmatrix},$$

$$s\equiv\begin{bmatrix}0 & 1\\ -1 & 0\end{bmatrix}\leftrightarrow i\begin{bmatrix}-1 & 0\\ 0 & 1\end{bmatrix},$$

$$\begin{bmatrix}1 & 0\\ r & 1\end{bmatrix}\leftrightarrow\begin{bmatrix}1+\frac{1}{2}ir & \frac{1}{2}ir\\ -\frac{1}{2}ir & 1-\frac{1}{2}ir\end{bmatrix}.$$

Next, Bargmann [2] (p. 590) defines a 2-1 onto homomorphism SU(1,1) → SO(2,1), as follows. With every point x = (x^0, x^1, x^2) of the Minkowski space with metric

$$x^2=(x^0)^2-(x^1)^2-(x^2)^2,$$

we associate a 2×2 Hermitian matrix

$$x\rightarrow X=\begin{bmatrix}x^0 & x^1-ix^2\\ x^1+ix^2 & x^0\end{bmatrix};$$

then the homomorphism associates $\pm W\in SU(1,1)$ with $r\in SO(2,1)$ where

$Y = W X W^+$ and $y = rx$. (4)

It is easily checked that under this homomorphism,

$$\pm\begin{bmatrix}ch\zeta/2 & sh\zeta/2\\ sh\zeta/2 & ch\zeta/2\end{bmatrix}\leftrightarrow\begin{bmatrix}ch\zeta & sh\zeta & 0\\ sh\zeta & ch\zeta & 0\\ 0 & 0 & 1\end{bmatrix}\equiv l_2(\zeta),$$

$$\pm\begin{bmatrix} ch\zeta/2 & ish\zeta/2 \\ -ish\zeta/2 & ch\zeta/2 \end{bmatrix} \leftrightarrow \begin{bmatrix} ch\zeta & 0 & -sh\zeta \\ 0 & 1 & 0 \\ -sh\zeta & 0 & ch\zeta \end{bmatrix} \equiv l_1(-\zeta),$$

$$\pm\begin{bmatrix} e^{-i\theta/2} & 0 \\ 0 & e^{i\theta/2} \end{bmatrix} \leftrightarrow \begin{bmatrix} 1 & 0 & 0 \\ 0 & \cos\theta & -\sin\theta \\ 0 & \sin\theta & \cos\theta \end{bmatrix} \equiv r_0(\theta),$$

$$\pm\begin{bmatrix} -i & 0 \\ 0 & i \end{bmatrix} \leftrightarrow \begin{bmatrix} 1 & 0 & 0 \\ 0 & -1 & 0 \\ 0 & 0 & -1 \end{bmatrix},$$

$$\pm\begin{bmatrix} 1+\frac{1}{2}ir & \frac{1}{2}ir \\ -\frac{1}{2}ir & 1-\frac{1}{2}ir \end{bmatrix} \leftrightarrow \begin{bmatrix} 1+\frac{1}{2}ir^2 & \frac{1}{2}ir^2 & -r \\ -\frac{1}{2}ir^2 & 1-\frac{1}{2}ir^2 & r \\ -r & -r & 1 \end{bmatrix}.$$

Combining the isomorphism (3) with the homomorphism (4), we get a 2-1 onto homomorphism

i: SL(2,R) ↔ SO(2,!) (5)

which gives the following associations:

$$\pm\begin{bmatrix} e^{\zeta/2} & 0 \\ 0 & e^{-\zeta/2} \end{bmatrix} \leftrightarrow \begin{bmatrix} ch\zeta & sh\zeta & 0 \\ sh\zeta & ch\zeta & 0 \\ 0 & 0 & 1 \end{bmatrix} \equiv l_2(\zeta),$$

$$\pm\begin{bmatrix} ch\zeta/2 & sh\zeta/2 \\ sh\zeta/2 & ch\zeta/2 \end{bmatrix} \leftrightarrow \begin{bmatrix} ch\zeta & 0 & -sh\zeta \\ 0 & 1 & 0 \\ -sh\zeta & 0 & ch\zeta \end{bmatrix} \equiv l_1(\zeta),$$

$$\pm\begin{bmatrix} \cos\theta/2 & \sin\theta/2 \\ -\sin\theta/2 & \cos\theta/2 \end{bmatrix} \leftrightarrow \begin{bmatrix} 1 & 0 & 0 \\ 0 & \cos\theta & -\sin\theta \\ 0 & \sin\theta & \cos\theta \end{bmatrix} \equiv r_0(\theta),$$

$$\pm s \equiv \pm\begin{bmatrix} 0 & 1 \\ -1 & 0 \end{bmatrix} \leftrightarrow \begin{bmatrix} 1 & 0 & 0 \\ 0 & -1 & 0 \\ 0 & 0 & -1 \end{bmatrix} \equiv s_0, \text{ say,}$$

$$\pm\begin{bmatrix}1 & 0\\ r & 1\end{bmatrix}\leftrightarrow\begin{bmatrix}1+\frac{1}{2}r^2 & \frac{1}{2}r^2 & -r\\ -\frac{1}{2}r^2 & 1-\frac{1}{2}r^2 & r\\ -r & -r & 1\end{bmatrix}\equiv t(r)\ ,\ \text{say.}$$

It therefore follows from Vilenkin's parameterization of SL(2,R) , that the general element of SO(2,1) can always be put in one of the following forms:

$$l_2(\xi)l_1(\zeta)l_2(\xi'),\ l_2(\xi)s_0l_1(\zeta)l_2(\xi'),\ l_2(\xi)r_0(\theta)l_2(\xi'),$$

$$l_2(\zeta)s_0r_0(\theta)l_2(\xi'),\ l_2(\xi)t(r)l_2(\xi'),\ l_2(\xi)s_0t(r)l_2(\xi'),$$

$$l_2(\xi)t(r)s_0l_2(\xi'),\ l_2(\xi)s_0t(r)s_0l_2(\xi').$$

As we are going to choose a basis in L ($H^{(1)}$) whose elements are eigenvectors of $l_2(\xi)$, we need to find out the matrix elements of the following operators only:

$$T_1^{\sigma}(\zeta)\equiv T^{\sigma}(l_1(\zeta)),\ T_{01}{}^{\sigma}(\zeta)\equiv T^{\sigma}(s_0l_1(\zeta)),\ T_0{}^{\sigma}(\theta)\equiv T^{\sigma}(r_0(\theta)),$$

$$T_{00}{}^{\sigma}(\theta)\equiv T^{\sigma}(s_0r_0(\theta)),\ T_t{}^{\sigma}(r)\equiv T^{\sigma}(t(r)),\ T_{0t}{}^{\sigma}(r)\equiv T^{\sigma}(s_0t(r)),$$

$$T_{t0}{}^{\sigma}(r)\equiv T^{\sigma}(t(r)s_0),\quad T_{0t0}{}^{\sigma}(r)\equiv T^{\sigma}(s_0t(r)s_0).$$

Note that the range of values of the variables ζ, θ and r are:

$-\infty<\zeta<\infty$, $-\pi/4\leq\theta<\pi/4$, $-\infty<r<\infty$.

The rest of the paper consists of evaluation of these matrix elements.

4. ACTION OF $T_1^{\sigma}(\zeta)$ ON $L^2(H^{(1)})$

When $g = l_1(\zeta)$,

$$g^{-1}=\begin{bmatrix}ch\zeta & 0 & -sh\zeta\\ 0 & 1 & 0\\ -sh\zeta & 0 & ch\zeta\end{bmatrix},$$

So, that

$$(g^{-1})_2{}^{\nu}\eta_{\nu} + (g^{-1})_2{}^{2} = (g^{-1})_2{}^{0}\eta_0 + (g^{-1})_2{}^{1}\eta_1 + (g^{-1})_2{}^{2} = -\eta_0 sh\zeta + ch\zeta = A,$$

$$(g^{-1})_0{}^{\nu}\eta_{\nu} + (g^{-1})_0{}^{2} = \eta_0 ch\zeta - sh\zeta,$$

$$(g^{-1})_1{}^{\nu}\eta_{\nu} + (g^{-1})_1{}^{2} = \eta_1 .$$

Hence, equation (2) will give

$$T_1^{\sigma}(\zeta) f(\eta_0, \eta_1) = \left|-\eta_0 sh\zeta + ch\zeta\right|^{\sigma} f\left(\frac{\eta_0 ch\zeta - sh\zeta}{A}, \frac{\eta_1}{A}\right)$$

$$= \left|-\eta_0 sh\zeta + ch\zeta\right|^{\sigma} f(\eta_0', \eta_1') \qquad (6)$$

Where,

$$\eta_0' = \frac{\eta_0 ch\zeta - sh\zeta}{A},\ \eta_1' = \frac{\eta_1}{A}.$$

Introduce now "spherical polar coordinates" φ, τ , on the hyperboloid $H^{(1)}$, by setting

$\eta_0 = \tau$ ch φ, $\eta_1 = \tau$sh φ, $-\infty < \phi < \infty$, τ= + or - ,

ch$\varphi = \tau\eta_0$, sh$\varphi = \tau\eta_1$, (7)

τ being a "labeling parameter" which distinguishes the upper and lower sheets of the hyperboloid $H^{(1)}$, and then change the independent variables in (6) from η_0 , η_1 to φ, τ. Then as η_0 , η_1 , change to η_0', η_1' under the group action, φ, τ, change to φ' , τ', which are defined by (7) with primes everywhere; to find these latter in terms of φ, τ, we note that when τ=+,

$$\eta_0' = \frac{\eta_0 ch\zeta - sh\zeta}{ch\zeta - \eta_0 sh\zeta} = \frac{ch\phi.ch\zeta - sh\zeta}{ch\zeta - ch\phi.sh\zeta}, \qquad (8)$$

which is + ve or - ve i.e. τ' is + or -, according as

ch ζ - ch φ shζ > 0 or < 0, (9)

as the number

ch φ ch ζ - sh ζ

is always + ve . If we now simplify (9), after assuming, for the sake of definiteness, that

$\zeta > 0,$ (10)

We see that these inequalities are equivalent to

tanh $\frac{|\phi|}{2} < e^{-\zeta}$ or > $e^{-\zeta}$,

respectively. It therefore follows that when τ = +,

$\tau' =$ + or - according as $|\varphi| < \varphi_0$ or $|\varphi| > \varphi_0$ (11)

where $\varphi_0 > 0$ is defined by

tanh $\frac{\phi_0}{2} = e^{-\zeta}$ (12)

Next, to find φ' , we note that (7) with primes everywhere, (8) and

$$\eta_1' = \frac{\eta_1}{ch\zeta - \eta_0 sh\zeta} = \frac{sh\phi}{ch\zeta - ch\phi.sh\zeta}$$

will give

$$ch\phi' = \tau'\eta_0' = \left\{ \begin{array}{l} \frac{ch\phi.ch\zeta - sh\zeta}{ch\zeta - ch\phi.sh\zeta} \; when \; |\phi| < \phi_0, \\ -\frac{ch\phi.ch\zeta - sh\zeta}{ch\zeta - ch\phi.sh\zeta} \; when \; |\phi| > \phi_0, \end{array} \right\}$$

$$sh\phi' = \tau'\eta_1' = \left\{ \begin{array}{l} \frac{sh\phi}{ch\zeta - ch\phi.sh\zeta} \; when \; |\phi| < \phi_0, \\ -\frac{sh\phi}{ch\zeta - ch\phi.sh\zeta} \; when \; |\phi| > \phi_0, \end{array} \right\}$$

and so, we get

$\exp(\varphi') = \mathrm{ch}\,\varphi' + \mathrm{sh}\,\varphi'$

$$= \begin{Bmatrix} \dfrac{ch\phi.ch\zeta - sh\zeta + sh\phi}{ch\zeta - ch\phi.sh\zeta} when\,|\phi| < \phi_0, \\ -\dfrac{ch\phi ch\zeta - sh\zeta + sh\phi}{ch\zeta - ch\phi.sh\zeta} when\,|\phi| > \phi_0, \end{Bmatrix}$$

which, after some simplification gives

$\varphi' = \varphi_1$ where

$$\exp(\varphi_1) = \left| \frac{e^{\phi} - \tanh\,\zeta/2}{1 - e^{\phi}.\tanh\,\zeta/2} \right| \text{ for all } \varphi. \tag{13}$$

Thus, when $\eta_0 > 0$, (6) takes the form

$$T_1^{\sigma}(\zeta)\, f(\varphi, +) = \begin{Bmatrix} |ch\zeta - ch\phi.sh\zeta|^{\sigma} f(\phi_1, +) when\,|\phi| < \phi_0, \\ |ch\zeta - ch\phi.sh\zeta|^{\sigma} f(\phi_1, -) when\,|\phi| > \phi_0. \end{Bmatrix} \tag{14}$$

Let us now return back to the splitting of $L^{(2)}(H^{(1)})$ into the direct sum of $L^{(2)}(H_+^{(1)})$ and $L^{(2)}(H_-^{(1)})$. For $f \varepsilon L^{(2)}(H^{(1)})$, let us set

$$f = \begin{bmatrix} f_1 \\ f_2 \end{bmatrix},\ f_1 \varepsilon\ L^2(H_+^{(1)}), f_2\ \varepsilon\ L^2(H_-^{(1)}),$$

where

$f_1(\varphi) = f(\varphi, +)$, $\quad f_2(\varphi) = f(\varphi, -)$.

The scalar product of two elements f, g, $\varepsilon\ L^2(H^{(1)})$, will be

$$(f, g) = \left(\begin{bmatrix} f_1 \\ f_2 \end{bmatrix}, \begin{bmatrix} g_1 \\ g_2 \end{bmatrix} \right) = \int_{-\infty}^{\infty} \left\{ \Sigma_{i=1}^{2} f_i^{\times}(\phi) g_i(\phi) \right\} d\phi \tag{15}$$

In this new notation (13) can be written as

$$T^{\sigma}(\zeta)\begin{bmatrix} f(\phi) \\ 0 \end{bmatrix} = \begin{Bmatrix} \begin{bmatrix} |ch\zeta - ch\phi sh\zeta|^{\sigma} f(\phi_1) \\ 0 \end{bmatrix} when\ |\phi| < \phi_0, \\ \begin{bmatrix} 0 \\ |ch\zeta - ch\phi sh\zeta|^{\sigma} f(\phi_1) \end{bmatrix} when\ |\phi| > \phi_0. \end{Bmatrix} \quad (16)$$

The case τ = - turns out to be simpler than the previous one. Here we have

$$\eta_0' = \frac{\eta_0 ch\zeta - sh\zeta}{ch\zeta - \eta_0 sh\zeta} = -\frac{ch\phi ch\zeta + sh\zeta}{ch\zeta + ch\phi sh\zeta},$$

so that as

$\frac{ch\phi ch\zeta + sh\phi}{ch\zeta + ch\phi sh\zeta}$ is always > 0 for ζ>0,

we will have τ' = -. It follows that

$$ch\,\varphi' = \frac{ch\phi ch\zeta + sh\zeta}{ch\zeta + ch\phi sh\zeta},$$

moreover

$\eta_1' = \frac{\eta_1}{ch\zeta - \eta_0 sh\zeta}$ gives $\eta_1' = \frac{-sh\phi}{ch\zeta + ch\phi sh\zeta}$

so that

$$sh\,\varphi' = \frac{sh\phi}{ch\zeta + ch\phi sh\zeta}.$$

hence, we will have

$$exp(\varphi') = ch\,\phi' + sh\phi' = \frac{ch\phi ch\zeta + sh\zeta + sh\phi}{ch\zeta + ch\phi sh\zeta}$$

which leads to $\varphi' = \varphi_2$ where

$$\exp(\varphi_2) = \frac{e^{\phi} + \tanh\zeta/2}{1 + e^{\phi}\tanh\zeta/2} = \left|\frac{e^{\phi} + \tanh\zeta/2}{1 + e^{\phi}\tanh\zeta/2}\right| \tag{17}$$

Thus when $\tau = -$, (6) takes the form

$$T^{\sigma}(\zeta)\begin{bmatrix} 0 \\ f(\phi)\end{bmatrix} = \begin{bmatrix} 0 \\ |ch\zeta + ch\phi sh\zeta|^{\sigma} f(\phi_2)\end{bmatrix} \tag{16'}$$

Combining 16) and (16'), we get

$$T^{\sigma}(\zeta)\begin{bmatrix} f_1(\phi) \\ f_2(\phi)\end{bmatrix} = \begin{cases} \begin{bmatrix} |ch\zeta - ch\phi sh\zeta|^{\sigma} f_1(\phi_1) \\ |ch\zeta + ch\phi sh\zeta|^{\sigma} f_2(\phi_2)\end{bmatrix} when\ |\phi| < \phi_0, \\ \begin{bmatrix} 0 \\ |ch\zeta - ch\phi sh\zeta|^{\sigma} f_1(\phi_1) + |ch\zeta + ch\phi sh\zeta|^{\sigma} f_2(\phi_2)\end{bmatrix} when\ |\phi| > \phi_0, \end{cases} \tag{18}$$

where ϕ_1 *and* ϕ_2 are given by (13,17).

5. MATRIX ELEMENTS $T_1^{\sigma}(\zeta)$

In order to calculate the matrix elements of $T_1^{\sigma}(\zeta)$, we must first of all choose a suitable basis for the carrier space $L^2(H^{(1)})$; following Mukunda, we choose this basis as the set of eigen-functions

$$|\sigma, p, \tau\rangle = \frac{1}{\sqrt{4\pi}}\begin{bmatrix} \exp(ip\phi) \\ \tau\exp(ip\phi)\end{bmatrix}$$

of the operator $I_2(\xi)$ (and hence also of J_2), as is easily chekedby using equation (2). We next define, again with Mukunda, the matrix element of $I_1(\zeta)$ (note that $T_1^{\sigma}(\zeta) \equiv T^{\sigma}(I_1(\zeta))$) as

$$F^{\sigma}_{\tau'\tau}(p', p, \zeta) = \langle\sigma, p', \tau'|\, T_1^{\sigma}(\zeta)\,|\sigma\, p, \tau\rangle,$$

so that

$$F^{\sigma}_{\tau'\tau}(p', p, \zeta) = \frac{1}{4\pi}\left(\begin{bmatrix} \exp(ip'\phi) \\ \tau' \exp(ip'\phi) \end{bmatrix}, T_1^{\sigma} \begin{bmatrix} \exp(ip\phi) \\ \tau \exp(ip\phi) \end{bmatrix}\right);$$

then as, for $\zeta>0$,

$$T_1^{\sigma}(\zeta)\begin{bmatrix} \exp(ip\phi) \\ \tau \exp(ip\phi) \end{bmatrix}$$

$$= \left\{ \begin{matrix} \begin{bmatrix} |ch\zeta - ch\phi sh\zeta|^{\sigma} \exp(ip\phi_1) \\ |ch\zeta + ch\phi sh\zeta|^{\sigma} \tau \exp(ip\phi_2) \end{bmatrix}' & |\phi| < \phi_0 \\ \begin{bmatrix} 0 \\ |ch\zeta - ch\phi sh\zeta|^{\sigma} \exp(ip\phi_1) + |ch\zeta + ch\phi sh\zeta|^{\sigma} \tau \exp(ip\phi_2) \end{bmatrix}' & |\phi| > \phi_0 \end{matrix} \right\},$$

we shall have, using expressions (13) and (17) for φ_1 and φ_2 and (15) for scalar products,

$$F^{\sigma}_{\tau'\tau}(p', p, \zeta)$$

$$= \frac{1}{4\pi}\Big[\int_{|\phi|<\phi_0} d\phi \exp(-ip'\phi) |ch\zeta - ch\phi sh\zeta|^{\sigma} \left| \frac{e^{\phi} - \tanh \zeta/2}{1 - e^{\phi} \tanh \zeta/2} \right|^{ip}$$

$$+ \int_{|\phi|<\phi_0} d\phi \tau'\tau \exp(-ip'\phi) |ch\zeta + ch\phi sh\zeta|^{\sigma} \left| \frac{e^{\phi} + \tanh \zeta/2}{1 + e^{\phi} \tanh \zeta/2} \right|^{ip}$$

$$+ \int_{|\phi|>\phi_0} d\phi \tau' \exp(-ip'\phi) |ch\zeta - ch\phi sh\zeta|^{\sigma} \left| \frac{e^{\phi} - \tanh \zeta/2}{1 - e^{\phi} \tanh \zeta/2} \right|^{ip}$$

$$+ \int_{|\phi|>\phi_0} d\phi \tau'\tau \exp(-ip'\phi) |ch\zeta + ch\phi sh\zeta|^{\sigma} \left| \frac{e^{\phi} + \tanh \zeta/2}{1 + e^{\phi} \tanh \zeta/2} \right|^{ip} \Big]$$

$$= \frac{1}{4\pi}\Big[\int_{|\phi|<\phi_0} d\phi \exp(-ip') |ch\zeta - ch\phi sh\zeta|^{\sigma} \left| \frac{e^{\phi} - \tanh \zeta/2}{1 - e^{\phi} \tanh \zeta/2} \right|^{ip}$$

$$+\tau' \int_{|\phi|>\phi_0} d\phi \exp(-ip'\phi)\,|\,ch\zeta - ch\phi sh\zeta/2\,|^{\sigma}\,|\,\frac{e^{\phi}-\tanh\zeta/2}{1-e^{\phi}\tanh\zeta/2}\,|^{ip}$$

$$+\tau'\tau \int_{-\infty}^{\infty} d\phi \exp(-ip'\phi)\,|\,ch\zeta + ch\phi sh\zeta\,|^{\sigma}\,|\,\frac{e^{\phi}+\tanh\zeta/2}{1+e^{\phi}\tanh\zeta/2}\,|^{ip}\,].$$

To identify this with Mukunda's expression, we note that for $\tau = \tau' = +$, this becomes

$$F^{\sigma}_{++}(p', p, \zeta)$$

$$= \frac{1}{4\pi}\int_{-\infty}^{\infty} d\phi \exp(ip'\phi)\,|\,ch\zeta - ch\phi sh\zeta\,|^{\sigma}\,|\,\frac{e^{\phi}-\tanh\zeta/2}{1-e^{\phi}\tanh\zeta/2}\,|^{ip}$$

$$+\frac{1}{4\pi}\int_{-\infty}^{\infty} d\phi \exp(ip'\phi)\,|\,ch\zeta + ch\phi sh\zeta\,|^{\sigma}\,|\,\frac{e^{\phi}+\tanh\zeta/2}{1+e^{\phi}\tanh\zeta/2}\,|^{\sigma},$$

which is exactly the same as the expression for

$$F^{(s,0)}_{++}(p', p, \nu)$$

given by Mukunda in equation (1.18), p. 2094, second paper of reference 4, if we keep in mind the facts that our ϕ, ζ, σ, are q, ν, and (1/2 – is) respectively, of Mukunda. The identity of other $F^{\sigma}_{\tau'\tau}$ with the corresponding expressions of Mukunda, obtained in the form of integrals similar to the RHS of his equation (1.18), by using his equations (1.15 a, b, c), can be similarly established.

We do not attempt to evaluate these integrals as this has already been done by Mukunda. However, as we *are* going to evaluate the integrals and get the final results in cases not covered by him, we do write the final result in this case, in order to compare it with those in cases not covered by him. Thus we have

$$F^{\sigma}_{\tau'\tau}(p', p, \zeta) = \frac{1}{4\pi^2}\Gamma(1/2 + ip' - i\rho)\Gamma(1/2 - ip + i\rho)\Gamma(ip - ip') \times$$

$$[ch\pi(p-\rho) + \tau'\tau ch\pi(p'-\rho) + i\tau' sh\pi(p-p')](ch^2\zeta/2)^{i(p'+p)/2} \times$$

$$(sh^2\zeta/2)^{i(p'-p)/2} F(1/2 - i\rho + ip', 1/2 + i\rho + ip'; 1 + ip' - ip; -sh^2\zeta/2)$$

$+ [\tau\tau' \times \{p \leftrightarrow p', \rho \leftrightarrow -\rho$ in the first term$\}]$.

Note that the above expression corresponds to the case $\zeta>0$. When $\zeta<0$, calculations exactly similar to the above one, give us

$$F^{\sigma}_{\tau'\tau}(p', p, \zeta)$$

$$= \frac{1}{4\pi}\Big[\int_{-\infty}^{\infty} d\phi \exp(-ip'\phi)\,|ch\zeta - ch\phi sh\zeta|^{\sigma}\,\Big|\frac{e^{\phi} - \tanh\zeta/2}{1 - e^{\phi}\tanh\zeta/2}\Big|^{ip}$$

$$+ \tau \int_{|\phi|>\phi_0(-\zeta)} d\phi \exp(-ip'\phi)\,|ch\zeta + ch\phi sh\zeta|^{\sigma}\,\Big|\frac{e^{\phi} + \tanh\zeta/2}{1 + e^{\phi}\tanh\zeta/2}\Big|^{ip}$$

$$+ \tau\tau' \int_{|\phi|<\phi_0(-\zeta)} d\phi \exp(-ip'\phi)\,|ch\zeta + ch\phi sh\zeta|^{\sigma}\,\Big|\frac{e^{\phi} + \tanh\zeta/2}{1 + \tanh\zeta/2}\Big|^{ip}\Big] .$$

However, a much shorter way of obtaining this matrix element, which has the additional advantage of expressing it in terms of

$$F^{\sigma}_{\tau'\tau}(p', p, \zeta), \zeta > 0,$$

is, as indicated by Mukunda [4], as follows. As the representation T^{σ} is unitary, we will have

$$(T_1{}^{\sigma}(\zeta))^{+} = T_1{}^{\sigma}(-\zeta),$$

so that for $\zeta<0$,

$$F^{\sigma}_{\tau'\tau}(p', p, \zeta) = \langle \sigma, p', \tau' \mid T_1{}^{\sigma}(\zeta) \mid \sigma, p, \tau \rangle$$

$$= \langle \sigma, p, \tau \mid (T_1{}^{\sigma}(\zeta))^{+} \mid \sigma, p', \tau' \rangle^{\times}$$

$$= \langle \sigma, p, \tau \mid T_1{}^{\sigma}(-\zeta) \mid \sigma, p', \tau' \rangle^{\times}$$

This implies $F^{\sigma}_{\tau'\tau}(p', p, \zeta) = \{F^{\sigma}_{\tau\tau'}(p, p', -\zeta)\}^{\times}$ for $\zeta < 0$,

as asserted. Note that the integral representation of the RHS, obtained from that of $F^{\sigma}_{\tau'\tau}(p', p, \zeta)$, $\zeta > 0$, given earlier, is apparently different from the above explicit representation of the LHS; however, the identity of these two expressions is established in Appendix A. Moreover, the reason for obtaining the above explicit integral representation of $F^{\sigma}_{\tau'\tau}(p', p, \zeta)$, $\zeta<0$, when a simpler alternative expression for it is available, is that it enables us, as will be seen later, to express some other matrix element in terms of $F^{\sigma}_{\tau'\tau}(p', p, \zeta)$, $\zeta>0$

6. MATRIX ELEMENTS OF OTHER OPERATORS

We now compute the matrix elements of the other operators listed on pages 15-16. As the procedure for some of these computations is quite similar to that given above for the calculation of $F^{\sigma}_{\tau'\tau}$, we omit the details in these cases (in order to avoid repetition and to save space) and give only the important steps appearing there, and the final result.

I. $$T^{\sigma}_{01}(\zeta) \equiv T^{\sigma}(s_0 l_1(\zeta))$$

When $g=s_0 l_1(\zeta)$, direct multiplication of matrices gives

$$g^{-1}=\begin{bmatrix} ch\zeta & 0 & sh\zeta \\ 0 & -1 & 0 \\ -sh\zeta & 0 & -ch\zeta \end{bmatrix};$$

this, as in the above case, leads, when $\zeta>0$, to

$$T_{01}{}^{\sigma}(\zeta)\begin{bmatrix} f_1(\phi) \\ f_2(\phi) \end{bmatrix}$$

=

$$\left\{ \begin{bmatrix} |ch\zeta - ch\phi sh\zeta|^{\sigma} \; f_2(-\phi_1) \\ |ch\zeta + ch\phi sh\zeta|^{\sigma} \; f_1(-\phi_2) \end{bmatrix}, |\phi| < \phi_0 \right\}$$
$$\left\{ \begin{bmatrix} 0 \\ |ch\zeta + ch\phi sh\zeta|^{\sigma} \; f_1(-\phi_2) + |ch\zeta - ch\phi sh\zeta|^{\sigma} \; f_2(-\phi_1) \end{bmatrix}, |\phi| > \phi_0 \right\}$$

.

where φ_0, φ_1, φ_2 are as defined in equations (12), (13) and (17). It follows that

$$T_{01}{}^{\sigma}(\zeta)\begin{bmatrix} \exp(ip\phi) \\ \tau \exp(ip\phi) \end{bmatrix}$$

=

$$\left\{ \begin{bmatrix} |ch\zeta - ch\phi sh\zeta|^{\sigma} \; \tau \exp(-ip\phi_1) \\ |ch\zeta + ch\phi sh\zeta|^{\sigma} \; \exp(-ip\phi_2) \end{bmatrix}, |\phi| < \phi_0 \right\}$$
$$\left\{ \begin{bmatrix} 0 \\ |ch\zeta + ch\phi sh\zeta|^{\sigma} \; \exp(-ip\phi_2) + |ch\zeta - ch\phi sh\zeta|^{\sigma} \; \tau \exp(-ip\phi_1) \end{bmatrix}, |\phi| > \phi_0 \right\}$$

,

so that the matrix element

$$F^{0\sigma}_{\tau'\tau}(p', p, \zeta) = \frac{1}{4\pi}\left(\begin{bmatrix} \exp(ip'\phi) \\ \tau' \exp(ip'\phi \end{bmatrix}, T_{01}{}^{\sigma}(\zeta) \begin{bmatrix} \exp(ip\phi) \\ \tau \exp(ip\phi) \end{bmatrix} \right)$$

will have the expression

$$F^{0\sigma}_{\tau'\tau}(p', p, \zeta)$$

$$= \frac{1}{4\pi}[\tau \int_{|\phi|<\phi_0} d\phi \exp(-ip'\phi) \mid ch\zeta - ch\phi sh\zeta \mid^{\sigma} \mid \frac{e^{\phi} - \tanh \zeta/2}{1 - e^{\phi} \tanh \zeta/2} \mid^{-ip}$$

$$+\tau'\tau \int_{|\phi|>\phi_0} d\phi \exp(-ip'\phi) \mid ch\zeta - ch\phi sh\zeta \mid^{\sigma} \mid \frac{e^{\phi} - \tanh \zeta/2}{1 - e^{\phi} \tanh \zeta/2} \mid -ip$$

$$+\tau' \int_{-\infty}^{\infty} d\phi \exp(-ip'\phi) \mid ch\zeta + ch\phi sh\zeta \mid^{\sigma} \mid \frac{e^{\phi} + \tanh \zeta/2}{1 + e^{\phi} \tanh \zeta/2} \mid^{-ip}]$$

$$= \tau F^{\sigma}_{\tau'\tau}(p', -p, \zeta).$$

When $\zeta<0$, Mukunda's trick applied in the previous case, does not work, as here we have

$(T^{\sigma}_{01}(\zeta))^{-1} = T^{\sigma}_{01}(\zeta)$ in contrast to the relation $(T_1{}^{\sigma}(\zeta))^{-1} = T_1{}^{\sigma}(-\zeta)$;

we therefore have to repeat the whole calculation in this case, and we find that

$$F^{0\sigma}_{\tau'\tau}(p', p, \zeta) = \tau F^{\sigma}_{\tau'\tau}(p', -p, \zeta), \zeta<0,$$

(we have used the integral representation of the RHS obtained earlier) which gives

$$F^{0\sigma}_{\tau'\tau}(p', p, \zeta) = \tau \{F^{\sigma}_{\tau\tau'}(-p, p', -\zeta)\}^{\times}, \zeta<0.$$

II . $T_0{}^{\sigma}(\theta) \equiv T^{\sigma}(r_0(\theta))$.

Here $g=r_0(\theta)$, so that

$$g^{-1} = (r_0(\theta))^{-1} = \begin{bmatrix} 1 & 0 & 0 \\ 0 & \cos\theta & \sin\theta \\ 0 & -\sin\theta & \cos\theta \end{bmatrix}$$

this leads, when $\theta>0$ (recall that $-\pi/4<\theta<\pi/4$), to

$$T_0^{\sigma}(\theta)\begin{bmatrix} f(\phi) \\ 0 \end{bmatrix} = \left\{ \begin{bmatrix} |\cos\theta - sh\phi \sin\theta|^{\sigma} \; f(\phi_1{}') \\ 0 \end{bmatrix}, \phi < \phi_0{}' \right\}$$
$$\left\{ \begin{bmatrix} 0 \\ |\cos\theta - sh\phi \sin\theta|^{\sigma} \; f(\phi_1{}') \end{bmatrix}, \phi > \phi_0{}' \right\}$$

and

$$T_0^{\sigma}(\theta)\begin{bmatrix} 0 \\ f(\phi) \end{bmatrix} = \left\{ \begin{bmatrix} |\cos\theta + sh\phi \sin\theta|^{\sigma} \; f(\phi_2{}') \\ 0 \end{bmatrix}, \phi < -\phi_0{}' \right\}$$
$$\left\{ \begin{bmatrix} 0 \\ |\cos\theta + sh\phi \sin\theta|^{\sigma} \; f(\phi_2{}') \end{bmatrix}, \phi > -\phi_0{}' \right\}$$

where

$$\exp(\varphi_0{}') = \cot\theta/2, \tag{19 a}$$

$$\exp(\varphi_1{}') = \left| \frac{e^{\phi} + \tan\theta/2}{1 - e^{\phi}\tan\theta/2} \right|, \exp(\varphi_2{}') = \left| \frac{e^{\phi} - \tan\theta/2}{1 + e^{\phi}\tan\theta/2} \right| \tag{19 b}$$

We now write the matrix element

$$G^{\sigma}_{\tau'\tau}(p', p, \theta) = <\sigma, p', \tau' | T_0^{\sigma}(\theta) | \sigma, p, \tau>$$

$$= \frac{1}{4\pi}\left(\begin{bmatrix} \exp(ip'\phi) \\ \tau' \exp(ip'\kappa) \end{bmatrix}, T_0^{\sigma}(\theta) \begin{bmatrix} \exp(ip\phi) \\ \tau \exp(ip\phi) \end{bmatrix} \right)$$

in the form

$$\frac{1}{4\pi}\left(\begin{bmatrix} \exp(ip'\phi) \\ \tau' \exp(ip') \end{bmatrix}, T_0^{\sigma}(\theta) \begin{bmatrix} \exp(ip\phi) \\ 0 \end{bmatrix} \right) +$$

$$\frac{1}{4\pi}\left(\begin{bmatrix} \exp(ip'\phi) \\ \tau' \exp(ip'\phi) \end{bmatrix}, T_0^{\sigma}(\theta) \begin{bmatrix} 0 \\ \tau \exp(ip\phi) \end{bmatrix} \right)$$

and so get its value as

$G^{\sigma}_{\tau'\tau}(p', p, \theta)$

$$= \frac{1}{4\pi}\Big[\int_{-\infty}^{\phi_0'} d\phi \exp(-ip'\phi)\,|\cos\theta - sh\,\phi \sin\theta|^{\sigma}\,\Big|\frac{e^{\phi} + \tan\theta/2}{1 - e^{\phi}\tan\theta/2}\Big|^{ip}$$

$$+\tau'\int_{\phi_0'}^{\infty} d\phi \exp(-ip'\phi)\,|\cos\theta - sh\,\phi \sin\theta|^{\sigma}\,\frac{e^{\phi} + \tan\theta/2}{1 - e^{\phi}\tan\theta/2}\Big|^{ip}$$

$$+\tau\int_{-\infty}^{-\phi_0'} d\phi \exp(-ip'\phi)\,|\cos\theta + sh\,\phi \sin\theta|^{\sigma}\,\Big|\frac{e^{\phi} - \tan\theta/2}{1 + e^{\phi}\tan\theta/2}\Big|^{ip}$$

$$+\tau'\tau\int_{-\phi_0'}^{\infty} d\phi \exp(-ip'\phi)\,|\cos\theta + sh\,\phi \sin\theta|^{\sigma}\,\Big|\frac{e^{\phi} - \tan\theta/2}{1 + e^{\phi}\tan\theta/2}\Big|^{ip}\Big],$$

which is again identical, for $\tau' = \tau = +$, with the expression for $G^{(s,0)}_{++}(p', p, \mu)$ given by Mukunda in equation (1.21), p. 2095, second paper of reference (4), with the replacements -1/2 – is, q, μ, $\rightarrow \sigma$, φ, θ respectively

When $\theta<0$, we again have $(T_0{}^{\sigma}(\theta))^{+} = T_0{}^{\sigma}(-\theta)$, which leads, as before to

$$G^{\sigma}_{\tau'\tau}(p', p, \theta) = \{G^{\sigma}_{\tau\tau'}(p, p', -\theta)\}^{\times}, \theta<0,$$

but as in the case of $F^{\sigma}_{\tau'\tau}(p', p, \zeta), \zeta < 0$ we actually calculate its value also in terms of integrals and find that

$$G^{\sigma}_{\tau'\tau}(p', p, \theta)$$

$$= \frac{1}{4\pi}\Big[\int_{\phi_0'(-\theta)}^{\infty} d\phi \exp(-ip'\phi)\,|\cos\theta - sh\,\phi \sin\theta|^{\sigma}\,\Big|\frac{e^{\phi} + \tan\theta/2}{1 - e^{\phi}\tan\theta/2}\Big|^{ip}$$

$$+\tau' \int_{-\infty}^{\phi_0'(-\theta)} d\phi \exp(-ip'\phi) \mid \cos\theta - sh\phi \sin\theta \mid^{\sigma} \mid \frac{e^{\phi} + \tan\theta/2}{1 - e^{\phi}\tan\theta/2} \mid^{ip}$$

$$+\tau \int_{\phi_0'(-\theta)}^{\infty} d\phi \exp(-ip'\phi) \mid \cos\theta + sh\phi \sin\theta \mid^{\sigma} \mid \frac{e^{\phi} - \tan\theta/2}{1 + e^{\phi}\tan\theta/2} \mid^{ip}$$

$$+\tau\tau' \int_{-\infty}^{\phi_0'(-\theta)} d\phi \exp(-ip'\phi) \mid \cos\theta + sh\phi \sin\theta \mid^{\sigma} \mid \frac{e^{\phi} - \tan\theta/2}{1 + e^{\phi}\tan\theta/2} \mid^{ip}] \cdot$$

II. $T_{00}{}^{\sigma}(\theta) \equiv T^{\sigma}(s_0 r_0(\theta))$

When $g=s_0 r_0(\theta)$, we find that

$$g^{-1} = \begin{bmatrix} 1 & 0 & 0 \\ 0 & -\cos\theta & -\sin\theta \\ 0 & \sin\theta & -\cos\theta \end{bmatrix},$$

and this leads, when $\theta>0$, to

$$T_{00}{}^{\sigma}(\theta)\begin{bmatrix} f(\phi) \\ 0 \end{bmatrix} = \left\{ \begin{bmatrix} \mid sh\phi \sin\theta - \cos\theta \mid^{\sigma} f(-\phi_1') \\ 0 \end{bmatrix}, \phi > \phi_0' \right\},$$
$$\left\{ \begin{bmatrix} 0 \\ \mid sh\phi \sin\theta - \cos\theta \mid^{\sigma} f(-\phi_1') \end{bmatrix}, \phi < \phi_0' \right\}$$

$$T_{00}{}^{\sigma}(\theta)\begin{bmatrix} 0 \\ f(\phi) \end{bmatrix} = \left\{ \begin{bmatrix} \mid sh\phi \sin\theta + \cos\theta \mid^{\sigma} f(-\phi_2') \\ 0 \end{bmatrix}, \phi > -\phi_0' \right\},$$
$$\left\{ \begin{bmatrix} 0 \\ \mid sh\phi \sin\theta + \cos\theta \mid^{\sigma} f(-\phi_2') \end{bmatrix}, \phi < -\phi_0' \right\}$$

so that writing again the matrix element

$$G^{0\sigma}_{\tau'\tau}(p', p, \theta) = \frac{1}{4\pi} \left(\begin{bmatrix} \exp(ip'\phi) \\ \tau' \exp(ip'\phi) \end{bmatrix}, T_{00}{}^{\sigma}(\theta) \begin{bmatrix} \exp(ip\phi \\ \tau \exp(ip\phi \end{bmatrix} \right)$$

as

$$\frac{1}{4\pi}\left(\begin{bmatrix}\exp(ip'\phi)\\ \tau'\exp(ip'\phi)\end{bmatrix}, T_{00}{}^{\sigma}(\theta)\begin{bmatrix}\exp(ip\phi)\\ 0\end{bmatrix}\right)+\frac{1}{4\pi}\left(\begin{bmatrix}\exp(ip'\phi)\\ \tau'\exp(ip'\phi)\end{bmatrix}, T_{00}{}^{\sigma}(\theta)\begin{bmatrix}0\\ \tau\exp(ip\phi)\end{bmatrix}\right)$$

we will get its value as

$$\frac{1}{4\pi}[\int_{\phi_0'}^{\infty} d\phi \exp(-ip'\phi)\,|\,sh\phi\sin\theta-\cos\theta\}^{\sigma}\,|\frac{e^{\phi}+\tan\theta/2}{1-e^{\phi}\tan\theta/2}|^{-ip}$$

$$+\tau'\int_{-\infty}^{\phi_0'} d\phi \exp(-ip'\phi)\,|\,sh\phi\sin\theta-\cos\theta\,|^{\sigma}\,|\frac{e^{\phi}+\tan\theta/2}{1-e^{\phi}\tan\theta/2}|^{-ip}$$

$$+\tau\int_{-\phi_0'}^{\infty} d\phi \exp(-ip'\phi)\,|\,sh\phi\sin\theta+\cos\theta\,|^{\sigma}\,|\frac{e^{\phi}-\tan\theta/2}{1+e^{\phi}\tan\theta/2}|^{-ip}$$

$$+\tau'\tau\int_{-\infty}^{-\phi_0'} d\phi \exp(-ip'\phi)\,|\,sh\phi\sin\theta+\cos\theta\,|^{\sigma}\,|\frac{e^{\phi}-\tan\theta/2}{1+e^{\phi}\tan\theta/2}|^{-ip}]$$

$$=\tau' G^{\sigma}_{\tau'\tau}(p', -p, \theta).$$

When $\theta<0$, we have, again, to repeat the whole calculation; we find that

$$G^{0\sigma}_{\tau'\tau}(p', p, \theta)=\tau' G^{\sigma}_{\tau'\tau}(p', -p, \theta)=\tau'\{G^{\sigma}_{\tau\tau'}(-p, p', -\theta)\}^{\times}$$

III. $$T^{\sigma}_{t}(r)\equiv T^{\sigma}(t(r))$$

As calculations in this case are somewhat different from those in the previous cases, we give them in some detail.

When g=t(r), we have

$$g^{-1} = \begin{bmatrix} 1+\frac{1}{2}r^2 & \frac{1}{2}r^2 & r \\ -\frac{1}{2}r^2 & 1-\frac{1}{2}r^2 & -r \\ r & r & 1 \end{bmatrix},$$

so that

$$(g^{-1})_2{}^{\nu}\,\eta_\nu + (g^{-1})_2{}^{2} = r\eta_0 + r\eta_1 + 1,$$

$$(g^{-1})_0{}^{\nu}\,\eta_\nu + (g^{-1})_0{}^{2} = (1+\frac{1}{2}r^2)\eta_0 + \frac{1}{2}r^2\eta_1 + r,$$

$$(g^{-1})_1{}^{\nu}\,\eta_\nu + (g^{-1})_1{}^{2} = -\frac{1}{2}r^2\eta_0 + (1-\frac{1}{2}r^2)\eta_1 - r,$$

Hence

$$T_t{}^{\sigma}(r) f(\eta_0, \eta_1) = |\, r\eta_0 + r\eta_1 + 1\,|^{\sigma}\ f(\eta_0{}', \eta_1{}') \qquad (20)$$

where

$$\eta_0{}' = \frac{(1+\frac{1}{2}r^2)\eta_0 + \frac{1}{2}r^2\eta_1 + r}{r\eta_0 + r\eta_1 + 1},\quad \eta_1{}' = \frac{-\frac{1}{2}r^2\eta_0 + (1-\frac{1}{2}r^2)\eta_1 - r}{r\eta_0 + r\eta_1 + 1}$$

In terms of the spherical polar coordinates τ, φ, these take, for τ=+, the form

$$\eta_0{}' = \frac{(1+\frac{1}{2}r^2)ch\phi + \frac{1}{2}r^2 sh\phi + r}{rch\phi + rsh\phi + 1} = \frac{1}{2}\frac{e^{\phi} + e^{-\phi}(re^{\phi}+1)^2}{re^{\phi}+1},$$

$$\eta_1{}' = \frac{-\frac{1}{2}r^2 ch\phi + (1-\frac{1}{2}r^2)sh\phi - r}{rch\phi + rsh\phi + 1} = \frac{1}{2}\frac{e^{\phi} - e^{-\phi}(re^{\phi}+1)^2}{re^{\phi}+1},$$

after some straight forward simplification. Hence, when r > 0 , $\eta_0{}' > 0 \Rightarrow \tau' = +$, and so

$$ch\phi' = \tau'\eta_0' = \frac{1}{2}\frac{e^{\phi} + e^{-\phi}(re^{\phi}+1)^2}{re^{\phi}+1},$$

$$sh\phi' = \tau'\eta_1' = \frac{1}{2}\frac{e^{\phi} - e^{-\phi}(re^{\phi}+1)^2}{}$$

$$\Rightarrow \exp(\phi') = ch\phi' + sh\phi' = \frac{e^{\phi}}{re^{\phi}+1} = \exp(\varphi_1'')\text{, say} \qquad (21a)$$

As $r\eta_0 + r\eta_1 + 1 = re^{\phi} + 1$, it follows that equation (20) leads to

$$T_t^{\sigma}(r)\begin{bmatrix} f(\phi) \\ 0 \end{bmatrix} = \begin{bmatrix} |re^{\phi}+1|^{\sigma} f(\phi_1'') \\ 0 \end{bmatrix}.$$

For τ= - , we shall have

$$\eta_0' = \frac{-(1+\frac{1}{2}r^2)ch\phi - \frac{1}{2}r^2 sh\phi + r}{-rch\phi - rsh\phi + 1} = \frac{1}{2}\frac{e^{\phi} + e^{-\phi}(re^{\phi}-1)^2}{re^{\phi}-1}$$

which is +ve or -ve i.e. τ'=+ or - according as

$re^{\varphi} - 1 > 0$ or < 0 i.e. as $\phi > \phi_0''$ or $\phi < \phi_0''$

where, $\exp(\varphi_0'') = \frac{1}{r} = |\frac{1}{r}|$ (22)

Next

$$\eta_1' = \frac{\frac{1}{2}r^2 ch\phi - (1-\frac{1}{2}r^2)sh\phi - r}{-rch\phi - rsh\phi + 1} = \frac{1}{2}\frac{-e^{\phi} + e^{-\phi}(re^{\phi}-1)^2}{1-re^{\phi}},$$

so that

$$ch\phi' = \tau' \eta_0' = \left\{ \begin{array}{l} \frac{1}{2}\frac{e^{\phi} + e^{-\phi}(re^{\phi}-1)^2}{re^{\phi}-1}, \phi > \phi_0'', \\ -\frac{1}{2}\frac{e^{\phi} + e^{-\phi}(re^{\phi}-1)^2}{re^{\phi}-1}, \phi < \phi_0'', \end{array} \right\}$$

$$sh\phi' = \tau' \eta_1' = \left\{ \begin{array}{l} \frac{1}{2}\frac{-e^{\phi} + e^{-\phi}(re^{\phi}-1)^2}{1-re^{\phi}}, \phi > \phi_0'', \\ -\frac{1}{2}\frac{-e^{\phi} + e^{-\phi}(re^{\phi}-1)^2}{1-re^{\phi}}, \phi < \phi_0'', \end{array} \right\}$$

$$\Rightarrow \exp(\phi') = \left\{ \begin{array}{l} \frac{e^{\phi}}{re^{\phi}-1}, \phi > \phi_0'' \\ -\frac{e^{\phi}}{re^{\phi}-1} \phi < \phi_0'' \end{array} \right\} = \left| \frac{e^{\phi}}{re^{\phi}-1} \right|, \forall \phi = \exp(\phi_2''), \text{ say} \qquad (21b)$$

As now $r\eta_0 + r\eta_1 + 1 = -rch\,\phi - rsh\,\phi + 1 = 1 - re^{\phi}$, we get

$$T_t^{\sigma}(r) \begin{bmatrix} 0 \\ f(\phi) \end{bmatrix} = \left\{ \begin{array}{l} \begin{bmatrix} |1-re^{\phi}|^{\sigma} f(\phi_2'') \\ 0 \end{bmatrix}, \phi > \phi_0'', \\ \begin{bmatrix} 0 \\ |1-re^{\phi}|^{\sigma} f(\phi_2'') \end{bmatrix}, \phi < \phi_0'', \end{array} \right\},$$

so that

$$T_t^{\sigma}(r) \begin{bmatrix} f_1(\phi) \\ f_2(\phi) \end{bmatrix} = \left\{ \begin{array}{l} \begin{bmatrix} |re^{\phi}+1|^{\sigma} f_1(\phi_1'') + |1-re^{\phi}|^{\sigma} f_2(\phi_2'') \\ 0 \end{bmatrix}, \phi > \phi_0'', \\ \begin{bmatrix} |re^{\phi}+1|^{\sigma} f_1(\phi_1'') \\ |1-re^{\phi}|^{\sigma} f_2(\phi_2'') \end{bmatrix}, \phi < \phi_0'', \end{array} \right\}.$$

Now the matrix element of $T_t^{\sigma}(r)$ is given by

$$T^{\sigma}_{\tau'\tau}(p', p, r) = < \sigma, p', \tau' | T_t^{\sigma}(r) | \sigma, p, \tau >$$

$$= \frac{1}{4\pi} \left(\begin{bmatrix} \exp(ip'\phi) \\ \tau' \exp(ip'\phi) \end{bmatrix}, T_t^{\sigma}(r) \begin{bmatrix} \exp(ip\phi) \\ \tau \exp(ip\phi) \end{bmatrix} \right),$$

so that as

$$T_t^{\sigma}(r)\begin{bmatrix} e^{ip\phi} \\ \tau e^{ip\phi} \end{bmatrix} = \left\{ \begin{bmatrix} |re^{\phi}+1|^{\sigma}\exp(ip\phi_1'') + |1-re^{\phi}|^{\sigma}\tau\exp(ip\phi_2'') \\ 0 \end{bmatrix}, \phi > \phi_0'' \right\}$$
$$\left\{ \begin{bmatrix} |re^{\phi}+1|^{\sigma}\exp(ip\phi_1'') \\ |1-re^{\phi}|^{\sigma}\tau\exp(ip\phi_2'') \end{bmatrix}, \phi < \phi_0'' \right\},$$

we will get

$$T_{\tau'\tau}^{\sigma}(p', p, r) = \frac{1}{4\pi}\Big[\int_{-\infty}^{\infty} d\phi \exp(-ip'\phi)\,|re^{\phi}+1|^{\sigma}\,\Big|\frac{e^{\phi}}{1+re^{\phi}}\Big|^{ip}$$

$$+ \int_{\phi<\phi_0''} d\phi\tau'\tau\exp(-ip'\phi)\,|1-re^{\phi}|^{\sigma}\,\Big|\frac{e^{\phi}}{1-re^{\phi}}\Big|^{ip}$$

$$+ \int_{\phi>\phi_0''} d\phi\tau\exp(-ip'\phi)\,|1-re^{\phi}|^{\sigma}\,\Big|\frac{e^{\phi}}{1-re^{\phi}}\Big|^{ip}\Big]$$

$$= \frac{1}{4\pi}\Big[\int_0^{\infty}(1+rx)^{\sigma-ip}x^{i(p-p')-1}dx + \tau'\tau\int_o^{1/r}(1-rx)^{\sigma-ip}x^{i(p-p'-1}dx$$

$$+\tau\int_{1/r}^{\infty}\{-(1-rx)\}^{\sigma-ip}x^{i(p-p')-1}dx\Big]\,,\ x=e^{\varphi}.$$

These integrals are evaluated in the Appendix B; substituting their values from there, we get, for r>0

$$T_{\tau'\tau}^{\sigma}(p', p, r) = \Big[\frac{\Gamma(i(p-p'))\Gamma(1/2-i\rho+ip')}{\Gamma(1/2-i\rho+ip)}$$

+

$$\tau'\tau\frac{\Gamma(i(p-p'))\Gamma(1/2+i\rho-ip)}{\Gamma(1/2+i\rho-ip')} + \tau\frac{\Gamma(1/2-i\rho+ip')\Gamma(1/2+i\rho-ip)}{\Gamma(1+i(p'-p)}\Big]$$

$r^{-i(p-p'}$.

Note the extreme simplicity of this expression as compared to that of

$F^{\sigma}_{\tau'\tau}(p', p, \zeta), \zeta > 0,$

given on pages 32-33; here, we simply get a multiple of power of r.

When r<0, we again have $\{T_t^{\sigma}(r)\}^{+} = T_t^{\sigma}(-r)$, and this leads to

$$T^{\sigma}_{\tau'\tau}(p', p, r) = \{T^{\sigma}_{\tau\tau'}(-r)\}^{\times}.$$

However, we find its value also in terms of integrals, by direct evaluation, and we get

$$T^{\sigma}_{\tau'\tau}(p', p, r) = \frac{1}{4\pi}[\tau\tau' \int_{-\infty}^{\infty} d\phi \exp(-ip'\phi) |1 - re^{\phi}|^{\sigma} |\frac{e^{\phi}}{1 - re^{\phi}}|^{ip}$$

$$+ \int_{\phi_0''(-r)}^{\infty} d\phi \exp(-ip'\phi) |1 + re^{\phi}|^{\sigma} |\frac{e^{\phi}}{1 + re^{\phi}}|^{ip}$$

$$+ \tau' \int_{-\infty}^{\phi_0''(-r)} d\phi \exp(-ip'\phi) |1 + re^{\phi}|^{\sigma} |\frac{e^{\phi}}{1 + re^{\phi}}|^{ip}].$$

V. $T^{0\sigma}_{t}(r) \equiv T^{\sigma}(s_0 t(r))$.

When $g = s_0 t(r)$, we find that

$$g^{-1} = \begin{bmatrix} 1 + 1/2r^2 & -1/2r^2 & -r \\ -1/2r^2 & -1 + 1/2r^2 & r \\ r & -r & -1 \end{bmatrix},$$

and this leads, as in the previous case, to

$$T^{0\sigma}_{t}(r) \begin{bmatrix} f_1(\phi) \\ f_2(\phi) \end{bmatrix}$$

$$= \begin{cases} \begin{bmatrix} |re^{-\phi}-1|^{\sigma} f_1(\phi_2''(-\phi)) + |re^{-\phi}+1|^{\sigma} f_2(\phi_1''(-\phi)) \\ 0 \end{bmatrix}, \phi < -\phi_0'' \\ \begin{bmatrix} |re^{-\phi}+1|^{\sigma} f_2(\phi_1''(-\phi) \\ |re^{-\phi}-1|^{\sigma} f_1(\phi_2''(-\phi) \end{bmatrix}, \phi > -\phi_0'' \end{cases},$$

when r>0. This, in turn, enables us to get the matrix elements of $T^{0\sigma}_{t}(r)$ as

$$T^{0\sigma}_{\tau'\tau}(p', p, r) = \frac{1}{4\pi}\left(\begin{bmatrix} \exp(ip'\phi) \\ \tau' \exp(ip'\phi) \end{bmatrix}, T^{0\sigma}_{t}(r) \begin{bmatrix} \exp(ip\phi \\ \tau \exp(ip\phi) \end{bmatrix} \right)$$

$$= \frac{1}{4\pi}[\int_{-\infty}^{-\phi_0''} d\phi \exp(-ip'\phi) |re^{-\phi}-1|^{\sigma} |\frac{e^{-\phi}}{re^{-\phi}-1}|^{ip}$$

$$+\tau' \int_{-\phi_0''}^{\infty} d\phi \exp(-ip'\phi) |re^{-\phi}-1|^{\sigma} |\frac{e^{-\phi}}{re^{-\phi}-1}|^{ip}$$

$$+\tau \int_{-\infty}^{\infty} d\phi \exp(-ip'\phi) |re^{-\phi}+1|^{\sigma} |\frac{e^{-\phi}}{re^{-\phi}+1}|^{ip}]$$

$$= \frac{1}{4\pi}[\tau \int_{-\infty}^{\infty} d\phi \exp(ip'\phi) |re^{\phi}+1|^{\sigma} |\frac{e^{\phi}}{re^{\phi}+1}|^{ip}$$

$$+ \int_{\phi_0''}^{\infty} d\phi \exp(ip'\phi) |re^{\phi}-1|^{\sigma} |\frac{e^{\phi}}{re^{\phi}-1}|^{ip}$$

$$+\tau' \int_{-\infty}^{\phi_0''} d\phi \exp(ip'\phi) |re^{\phi}-1|^{\sigma} |\frac{e^{\phi}}{re^{\phi}-1}|^{ip}]$$

by replacing φ by - φ as the variable of integration. It is now easy to check that

$$T^{0\sigma}_{\tau'\tau}(p', p, r) = \tau T^{\sigma}_{\tau'\tau}(-p', p, r) \text{ , r>0.}$$

When r<0, we have to repeat the whole calculation and we find that

$$T^{0\sigma}_{\tau'\tau}(p', p, r) = \tau T^{\sigma}_{\tau'\tau}(-p', p, r), \quad r<0,$$

$$= \tau\{T^{\sigma}_{\tau\tau'}(p, -p', -r)\}^{\times}, \quad r<0.$$

VI. $$T^{\sigma 0}_{t}(r) \equiv T^{\sigma}(t(r)s_0)$$

When $g = t(r)s_0$, we find that

$$g^{-1} = \begin{bmatrix} 1+\frac{1}{2}r^2 & \frac{1}{2}r^2 & r \\ \frac{1}{2}r^2 & -1+\frac{1}{2}r^2 & r \\ -r & -r & -1 \end{bmatrix}$$

which ultimately leads, for $r>0$, to

$$T^{\sigma 0}_{\tau'\tau}(p', p, r) = \tau' T^{\sigma}_{\tau'\tau}(p', -p, r),$$

and for $r<0$, to

$$T^{\sigma 0}_{\tau'\tau}(p', p, r) = \tau' T^{\sigma}_{\tau'\tau}(p', -p, r) = \tau'\{T^{\sigma}_{\tau\tau'}(-p, p', -r)\}^{\times}.$$

VII. $$T^{0\sigma 0}_{t}(r) \equiv T^{\sigma}(s_0 t(r) s_0).$$

Finally, when $g = s_0 t(r) s_0$, we have

$$g^{-1} = \begin{bmatrix} 1+\frac{1}{2}r^2 & -\frac{1}{2}r^2 & -r \\ \frac{1}{2}r^2 & 1-\frac{1}{2}r^2 & -r \\ -r & r & 1 \end{bmatrix},$$

which, as usual, leads, for r>0, to

$$T^{0\sigma 0}_{\tau'\tau}(p', p, r) = \tau'\tau\, T^{\sigma}_{\tau'\tau}(-p', -p, r)$$

and for r<0, to

$$T^{0\sigma 0}_{\tau'\tau}(p', p, r) = \tau'\tau\, T^{\sigma}_{\tau'\tau}(-p', -p, r) = \tau'\tau\{T^{\sigma}_{\tau\tau'}(-p, -p', -r)\}^{\times}.$$

7. CONCLUSIONS

We may conclude by saying that in order to find the matrix elements of an ARBITRARY rotation of SO(2, 1) in a unitary irreducible representation of principal series and of integral type, we have to consider 16 different cases corresponding to the 8 possible parametrisations given on pp. 15 and 16, with +ve and -ve arguments with each of them. These have all been computed and, luckily, we find that only 3 of them viz.

$$F^{\sigma}_{\tau'\tau}(p', p, \zeta), \zeta>0,$$

$$G^{\sigma}_{\tau'\tau}(p', p, \theta), \theta>0,$$

$$T^{\sigma}_{\tau'\tau}(p', p, r), r>0$$

are the basic or fundamental ones as the rest of 13 matrix elements can be expressed in terms of these 3. In order to clearly visualize this situation, we end up by explicitly listing the expressions for these 13 matrix elements in terms of these basic ones.

$$F^{\sigma}_{\tau'\tau}(p', p, \zeta) = \{F^{\sigma}_{\tau\tau'}(p, p', -\zeta)\}^{\times}, \zeta<0,$$

$$F^{0\sigma}_{\tau'\tau}(p', p, \zeta) = \tau F^{\sigma}_{\tau'\tau}(p', -p, \zeta), \zeta>0,$$

$$F^{0\sigma}_{\tau'\tau}(p',p,\zeta)=\tau F^{\sigma}_{\tau'\tau}(p',-p,\zeta)=\tau\{F^{\sigma}_{\tau\tau'}(-p,p',-\zeta)\}^{\times},\zeta<0,$$

$$G^{\sigma}_{\tau'\tau}(p',p,\theta)=\{G^{\sigma}_{\tau\tau'}(p,p',-\theta)\}^{\times},\theta<0,$$

$$G^{0\sigma}_{\tau'\tau}(p',p,\theta)=\tau' G^{\sigma}_{\tau'\tau}(p',-p,\theta),\theta>0,$$

$$G^{0\sigma}_{\tau'\tau}(p',p,\theta)=\tau' G^{\sigma}_{\tau'\tau}(p',-p,\theta)=\tau'\{G^{\sigma}_{\tau\tau'}(-p,p',-\theta)\}^{\times},\theta<0,$$

$$T^{\sigma}_{\tau'\tau}(p',p,r)=\{T^{\sigma}_{\tau\tau'}(p,p',-r)\}^{\times},r<0,$$

$$T^{0\sigma}_{\tau'\tau}(p',p,r)=\tau T^{\sigma}_{\tau'\tau}(-p',p,r),r>0,$$

$$T^{0\sigma}_{\tau'\tau}(p',p,r)=\tau T^{\sigma}_{\tau'\tau}(-p',p,r)=\tau\{T^{\sigma}_{\tau\tau'}(p,-p',-r)\}^{\times},r<0,$$

$$T^{\sigma 0}_{\tau'\tau}(p',p,r)=\tau' T^{\sigma}_{\tau'\tau}(p',-p,r),r>0,$$

$$T^{\sigma 0}_{\tau'\tau}(p',p,r)=\tau' T^{\sigma}_{\tau'\tau}(p',-p,r)=\tau'\{T^{\sigma}_{\tau\tau'}(-p,p',-r)\}^{\times},r<0,$$

$$T^{0\sigma 0}_{\tau'\tau}(p',p,r)=\tau\tau' T^{\sigma}_{\tau'\tau}(-p',-p,r),r>0,$$

$$T^{0\sigma 0}_{\tau'\tau}(p',p,r)=\tau\tau' T^{\sigma}_{\tau'\tau}(-p',-p,r)=\tau\tau'\{T^{\sigma}_{\tau\tau'}(-p,-p',-r)\}^{\times},r<0.$$

APPENDIX A

Here we establish the identity of the integral expressions for

$F^{\sigma}_{\tau'\tau}(p', p, \zeta)$ and $\{F^{\sigma}_{\tau\tau'}(p, p', -\zeta)\}^{\times}$

when $\zeta<0$, which was asserted in the text. We have (recall that $\tanh\frac{\phi_0(-\zeta)}{2} = e^{\zeta}$),

$$\{F^{\sigma}_{\tau\tau'}(p, p', -\zeta)\}^{\times}$$

=

$$\frac{1}{4\pi}\Big[\int_{|\phi|<\phi_0(-\zeta)} d\phi \exp(ip\phi)\,|\,ch\zeta + ch\phi sh\zeta\,|^{-1/2-i\rho}\,\Big|\frac{e^{\phi}+\tanh\zeta/2}{1+e^{\phi}\tanh\zeta/2}\Big|^{-ip'}$$

$$\tau\int_{|\phi|>\phi_0(-\zeta)} d\phi \exp(ip\phi)\,|\,ch\zeta + ch\phi sh\zeta\,|^{-1/2-i\rho}\,\Big|\frac{e^{\phi}+\tanh\zeta/2}{1+e^{\phi}\tanh\zeta/2}\Big|^{-ip}$$

$$\tau\tau'\int_{-\infty}^{\infty} d\phi \exp(ip\phi)\,|\,ch\zeta - ch\phi sh\zeta\,|^{-1/2-i\rho}\,\Big|\frac{e^{\phi}-\tanh\zeta/2}{1-e^{\phi}\tanh\zeta/2}\Big|^{-ip}\Big]$$

=

$$\frac{(1-t^2)^{1/2+i\rho}}{4\pi}\Big[\int_{-\phi_0(-\zeta)}^{\phi_0(-\zeta)} d\phi \exp(ip\phi)\,\Big|\frac{(e^{\phi}-t)(1-te^{\phi})}{e^{\phi}}\Big|^{-1/2-i\rho}\,\Big|\frac{e^{\phi}-t}{1-te^{\phi}}\Big|^{-ip'}$$

$$+\tau\int_{-\infty}^{-\phi_0(-\zeta)} d\phi \exp(ip\phi)\,\Big|\frac{(e^{\phi}-t)(1-te^{\phi})}{e^{\phi}}\Big|^{-1/2-i\rho}\,\Big|\frac{e^{\phi}-t}{1-te^{\phi}}\Big|^{-ip'}$$

$$+\tau\int_{\phi_0(-\zeta)}^{\infty} d\phi \exp(ip\phi)\,\Big|\frac{(e^{\phi}-t)(1-te^{\phi})}{e^{\phi}}\Big|^{-1/2-i\rho}\,\Big|\frac{e^{\phi}-t}{1-te^{\phi}}\Big|^{-ip'}$$

$$+\tau\tau'\int_{-\infty}^{\infty} d\phi \exp(ip\phi)\,\Big|\frac{(e^{\phi}+t)(1+te^{\phi})}{e^{\phi}}\Big|^{-1/2-i\rho}\,\Big|\frac{e^{\phi}+t}{1+te^{\phi}}\Big|^{-ip'}\Big]$$

where t=-tanh ζ/2>0, and we have used the easily verifiable facts that

$$ch\zeta + ch\phi sh\zeta = \frac{e^{-\phi}}{1-t^2}(e^{\phi} - t)(1 - te^{\phi}),$$

$$ch\zeta - ch\phi sh\zeta = \frac{e^{-\phi}}{1-t^2}(e^{\phi} + t)(1 + te^{\phi}).$$

Calling e^{φ} as x, we will have

$$dx = e^{\phi} d\phi \Rightarrow d\phi = \frac{dx}{x},$$

$$\phi < \phi_0(-\zeta) \Rightarrow e^{\phi} < e^{\phi_0(-\zeta)} = -\frac{1}{\tanh \zeta/2} = \frac{1}{t} \Rightarrow x < \frac{1}{t},$$

$$\phi > \phi_0(-\zeta) \Rightarrow x > \frac{1}{t},$$

$$\phi > -\phi_0(-\zeta) \Rightarrow e^{\phi} > e^{-\phi_0(-\zeta)} = t \Rightarrow x > t,$$

$$\phi < -\phi_0(-\zeta) \Rightarrow x < t,$$

$$\phi > -\infty \Rightarrow e^{\phi} > 0 \Rightarrow x > 0,$$

$$\phi < \infty \Rightarrow e^{\phi} < \infty \Rightarrow x < \infty,$$

so that the above expression will become

$$\frac{(1-t^2)^{1/2+i\rho}}{4\pi} \times \Big[\int_t^{1/t} \frac{dx}{x} x^{ip} \Big(\frac{(x-t)(1-tx)}{x}\Big)^{-1/2-i\rho} \Big(\frac{x-t}{1-tx}\Big)^{-ip'}$$

$$+ \tau \int_0^t \frac{dx}{x} x^{ip} \Big(\frac{(t-x)(1-tx)}{x}\Big)^{-1/2-i\rho} \Big(\frac{t-x}{1-tx}\Big)^{-ip'}$$

$$+ \tau \int_{1/t}^{\infty} \frac{dx}{x} x^{ip} \Big(\frac{(x-t)(tx-1)}{x}\Big)^{-1/2-i\rho} \Big(\frac{x-t}{tx-1}\Big)^{ip'}$$

$$+ \tau\tau' \int_0^{\infty} \frac{dx}{x} x^{ip} \Big(\frac{(x+t)(1+tx)}{x}\Big)^{-1/2-i\rho} \Big(\frac{x+t}{1+tx}\Big)^{ip'} \Big].$$

We now make a change of variable of integration from x to x', where

i) In the first integral, with t<x<1/t, we put

$x' = \frac{x-t}{1-tx}$ which gives $x = \frac{x'+t}{1+tx'}$, $1 - t\,x = \frac{1-t^2}{1+tx'}$, $\frac{x-t}{x} = (1-t^2)\frac{x'}{x'+t}$,

$dx = (1-t^2)\frac{dx'}{1+tx'}$, x=t$\rightarrow$ $x' = 0$, x=$\frac{1}{t} \rightarrow x' \rightarrow \infty$,

ii) in the second integral, with 0<x<t, we put

$$x' = \frac{t-x}{1-tx}$$

$$\Rightarrow x = \frac{t-x'}{1-tx'},\ 1 - tx = \frac{1-t^2}{1-tx'},\ \frac{t-x}{x} = (1-t^2)\frac{x'}{t-x'},$$

$$dx = -\frac{1-t^2}{(1-tx')^2},\ x=0 \rightarrow x' = t,\ x=t \rightarrow x' = 0,$$

iii) in the third integral, with 1/t<x<∞ , we put

$$x' = \frac{x-t}{tx-1}$$

$$\Rightarrow x = \frac{x'-t}{tx-1},\ tx-1 = \frac{1-t^2}{tx'-1},\ \frac{t-x}{x} = (1-t^2)\frac{x'}{x'-t},$$

$$dx = -\frac{1-t^2}{(tx'-1)^2}dx',\ x=1/t \rightarrow x' \rightarrow \infty,\ x \rightarrow \infty \rightarrow x' = 1/t,$$

iv) in the fourth integral, with 0<x<∞ , we put

$$x' = \frac{x+t}{1+tx}$$

$$\Rightarrow x = \frac{x'-t}{1-tx'},\ 1+tx = \frac{1-t^2}{1-tx'},\ \frac{x+t}{x} = (1-t^2)\frac{x'}{x'-t},$$

$$dx = \frac{1-t^2}{(1-tx')^2}dx',\ x = 0 \rightarrow x' = t,\ x \rightarrow \infty \rightarrow x' = 1/t.$$

Then the above expression will then transform to

$$\{F^{\sigma}_{\tau\tau'}(p,p',-\zeta)\}^{\times} = \frac{(1-t^2)^{1/2+i\rho}}{4\pi} \times$$

$$\Big[$$

$$\int_0^{\infty} dx' \, \frac{1-t^2}{(1+tx')^2} \Big(\frac{x'+t}{1+tx'}\Big)^{ip-1} \Big((1-t^2)\frac{x'}{x'+t}\cdot\frac{1-t^2}{1+tx'}\Big)^{-1/2-i\rho} (x')^{-ip'}$$

$$+$$

$$\tau\int_t^0 dx' \cdot -\frac{1-t^2}{(1-tx')^2} \Big(\frac{t-x'}{1-tx'}\Big)^{ip-1} \Big((1-t^2)\frac{x'}{t-x'}\cdot\frac{1-t^2}{1-tx'}\Big)^{-1/2-i\rho} (x')^{-ip'}$$

$$+$$

$$\tau\int_{\infty}^{1/t} dx' \cdot -\frac{1-t^2}{(tx'-1)^2} \Big(\frac{x'-t}{tx'-1}\Big)^{ip-1} \Big((1-t^2)\frac{x'}{x'-t}\cdot\frac{1-t^2}{tx'-1}\Big)^{-1/2-i\rho} (x')^{-ip'}$$

$$+$$

$$\tau\tau'\int_t^{1/t} dx' \, \frac{1-t^2}{(1-tx')^2} \Big(\frac{x'-t}{1-tx'}\Big)^{ip-1} \Big((1-t^2)\frac{x'}{x'-t}\cdot\frac{1-t^2}{1-tx'}\Big)^{-1/2-i\rho} (x')^{ip'} \Big]$$

$$= \frac{(1-t^2)^{1/2-i\rho}}{4\pi} \times$$

$$\Big[\int_0^{\infty} \frac{dx'}{x'} (x')^{-ip'} \Big|\frac{(x'+t)(1+tx')}{x'}\Big|^{-1/2+i\rho} \Big|\frac{x'+t}{1+tx'}\Big|^{ip}$$

$$+ \tau\int_0^{t} \frac{dx'}{x'} (x')^{-ip'} \Big|\frac{(t-x')(1-tx')}{x'}\Big|^{-1/2+i\rho} \Big|\frac{t-x'}{1-tx'}\Big|^{ip}$$

$$+ \tau\int_{1/t}^{\infty} \frac{dx'}{x'} (x')^{-ip'} \Big|\frac{(x'-t)(tx'-1)}{x'}\Big|^{-1/2+i\rho} \Big|\frac{x'-t}{tx'-1}\Big|^{ip}$$

$$+\tau\tau' \int_t^{1/t} \frac{dx'}{x'} (x')^{-ip'} \left| \frac{(x'-t)(1-tx')}{x'} \right|^{-1/2+i\rho} \left| \frac{x'-t}{1-tx'} \right|^{ip}]$$

$$= \frac{1}{4\pi} [\int_{-\infty}^{\infty} d\phi \exp(-ip'\phi) \left| ch\zeta - ch\phi sh\zeta \right|^{\sigma} \left| \frac{e^{\phi} - \tanh \zeta/2}{1 - e^{\phi} \tanh \zeta/2} \right|^{ip}$$

$$+\tau \int_{|\phi|>\phi_0(-\zeta)} d\phi \exp(-ip'\phi) \left| ch\zeta + ch\phi sh\zeta \right|^{\sigma} \left| \frac{e^{\phi} + \tanh \zeta/2}{1 + e^{\phi} \tanh \zeta/2} \right|^{ip}$$

$$+\tau\tau' \int_{|\phi|<\phi_0(-\zeta)} d\phi \exp(-ip'\phi) \left| ch\zeta + ch\phi sh\zeta \right|^{\sigma} \left| \frac{e^{\phi} + \tanh \zeta/2}{1 + e^{\phi} \tanh \zeta/2} \right|^{ip}]$$

(where now $x' = e^{\phi}$) which is identical with the explicit expression for

$F^{\sigma}_{\tau'\tau}(p', p, \zeta)$, $\zeta<0$,

given in the text.

APPENDIX B

Here we evaluate the integrals

$$\int_0^{\infty} (1+rx)^{\sigma-ip} x^{i(p-p')-1} dx, \quad \int_0^{1/r} (1-rx)^{\sigma-ip} x^{i(p-p')-1} dx,$$

$$\int_{1/r}^{\infty} \{-(1-rx)\}^{\sigma-ip} x^{i(p-p')-1} dx,$$

appearing in the text, in the expression for

$T^{\sigma}_{\tau'\tau}(p', p, r)$, r>0.

For the purpose, we simply use the formulas

1. $\int_0^{\infty} (1+ax)^{-\nu} x^{s-1} dx = a^{-s} B(s, \nu - s)$, $|\arg a|<\pi$, $0<\mathrm{Re}\, s<\mathrm{Re}\, \nu$,

2. $\int_0^b (1+ax)^{-\nu} x^{s-1} dx = s^{-1} b^s {}_2F_1(\nu, s; 1+s; -ab)$, |arg (1+ab)|<π , Re s>0,

3.

$$\int_b^\infty (1+ax)^{-\nu} x^{s-1} dx = a^{-\nu} b^{s-\nu} (\nu - s)^{-1} {}_2F_1(\nu, \nu - s; \nu - s + 1; -a^{-1}b^{-1})$$

,

Re s < Re ν , given in Erdelyi [9] . Thus, taking

$$\nu = -\sigma + ip = \frac{1}{2} - i(\rho - p) \text{ , s = i (p – p}'\text{),}$$

$$\Rightarrow \nu - s = \frac{1}{2} - i\rho + ip - ip + ip' = \frac{1}{2} - i(\rho - p'),$$

the first formula gives

$$\int_0^\infty (1+rx)^{\sigma - ip} x^{i(p-p')-1} dx$$

$$= r^{-i(p-p')} B(i(p-p'), \frac{1}{2} - i(\rho - p'))$$

$$= \frac{\Gamma(i(p-p'))\Gamma(\frac{1}{2} - i\rho + ip')}{\Gamma(\frac{1}{2} - i\rho + ip)} r^{-i(p-p')},$$

while the second formula gives

$$\int_0^{1/r} (1-rx)^{\sigma - ip} x^{i(p-p')} dx$$

$$= \frac{1}{i(p-p')} r^{-i(p-p')} {}_2F_1(\frac{1}{2} - i\rho + ip, i(p-p'); i(p+p') + 1; 1) \cdot$$

Now as

$${}_2F_1(a,b;c;1) = \frac{\Gamma(c)\Gamma(c-a-b)}{\Gamma(c-a)\Gamma(c-b)}$$, c ≠ 0, -1, -2, Re c>Re(a+b),

we will have

$${}_2F_1(\frac{1}{2} - i\rho + i$$

$$+ ip, i(p-p'); i(p-p')+1;1) = \frac{\Gamma(i(p-p')+1)\Gamma(\frac{1}{2}+i\rho-ip)}{\Gamma(\frac{1}{2}+i\rho-ip')},$$

so that

$$\int_0^{1/r} (1-rx)^{\sigma-ip} x^{i(p-p')-1} dx$$

$$= \frac{1}{i(p-p')} \frac{\Gamma(i(p-p')+1)\Gamma(\frac{1}{2}+i\rho-ip)}{\Gamma(\frac{1}{2}+i\rho-ip')} r^{-i(p-p')}$$

$$= \frac{\Gamma(i(p-p'))\Gamma(\frac{1}{2}+i\rho-ip)}{\Gamma(\frac{1}{2}+i-ip')} r^{-i(p-p')}.$$

Similarly, the third of the above formulas, gives

$$\int_{1/r}^{\infty} (-1)^{\sigma-ip} (1-rx)^{\sigma-ip} x^{i(p-p')} dx$$

$$= (-1)^{\sigma-ip} (-r)^{\sigma-ip} r^{-\sigma+ip-i(p-p')} \cdot \frac{1}{-\sigma+ip-i(p-p')} \times$$

$${}_2F_1(\frac{1}{2} - i\rho + ip, \frac{1}{2} - i\rho + ip - ip + ip'; \frac{1}{2} - i\rho + ip - ip + ip' + 1;1)$$

$$= \frac{1}{\frac{1}{2} - i\rho + ip'} r^{-i(p-p')} {}_2F_1(\frac{1}{2} - i\rho + ip, \frac{1}{2} - i\rho + ip'; \frac{3}{2} - i\rho + ip';1)$$

$$= \frac{1}{\frac{1}{2} - i\rho + ip'} \frac{\Gamma(\frac{3}{2} - i\rho + ip')\Gamma(\frac{1}{2} + i\rho - ip)}{\Gamma(1 + ip' - ip)} r^{-i(p-p')}$$

$$= \frac{\Gamma(\frac{1}{2} - i\rho + ip')\Gamma(\frac{1}{2} + i\rho - ip)}{\Gamma(1 + ip' - ip)} r^{-i(p-p')},$$

giving the required expressions for all the three integrals.

REFERENCES

1. E. P. Wigner, Grouppen Theorie, Vieweg Braunsohweig, New York Academic Press, (1931).
2. V. Bargmann, Ann. Math. 48 (1947) 568.
3. D. Basu and K. B. Wolf, J. Math. Phys., 23 (1982) 189.
4. N. Mukunda, J. Math. Phys. 10, 2086 (1969); N. Mukunda, J. Math. Phys. 10, 2092 (1969).
5. A. Syed, J. Math. Phys. 27, 1195 (1986).
6. C. P. Boyer and F. Ardalan, J. Math. Phys. 12 (1971) 2070.
7. N. Y. Vilenkin, Special Functions and Group Representation Theory, AMS Translations of Mathematical Monographs, (American Mathematical Society, Providence, Rhodes Island, 1968). Vol. 22; p. 369.
8. A. W. Knapp, Representation Theory of Semi-simple Groups, Princeton University Press, 2001; p. 39.
9. Harry Bateman and A. Erdelyi, Tables of Integral Transforms, (McGraw Hill, New York, 1954), Vol. I, p. 310.